

Thermodynamics of the q -deformed Kittel–Shore model

VÍCTOR MARISCAL¹ AND J. JAVIER RELANCIO^{1,2}

¹ Departamento de Matemáticas y Computación, Universidad de Burgos, 09001 Burgos, Spain

²Centro de Astropartículas y Física de Altas Energías (CAPA), Universidad de Zaragoza, Zaragoza 50009, Spain

e-mail: vmariscal@ubu.es, jjrelancio@ubu.es

Abstract

The Kittel–Shore Hamiltonian characterizes N spins with identical long-range interactions, and the $\mathfrak{su}(2)$ coalgebra has been proven to be a symmetry of this model, which can be exactly solved. By using quantum groups and, in particular, $\mathfrak{su}_q(2)$, this Hamiltonian was deformed. In this work, we study the thermodynamic properties of this deformed model for spin-1/2 particles. In particular, we discuss how this deformation affects the specific heat, magnetic susceptibility, magnetisation, and phase transitions as a function of the parameter q of the deformation and compare them with those of the undeformed model. Deformation was found to shift the thermodynamic behaviours to higher temperatures and alter the phase transitions. The potential applications of this q -deformed model for describing few-spin quantum systems with non-identical couplings are discussed.

PACS:

KEYWORDS: Kittel–Shore model; quantum algebras; integrability; spin systems; thermodynamics of spin chains

Contents

1	Introduction	2
2	The Kittel–Shore model and its q-deformation	3
3	The ferromagnetic case	5
3.1	Small number of spins	5
3.2	Thermodynamic limit	7
3.2.1	Thermodynamic properties	7
3.3	q -deformation for small number of spins	9
3.4	q -deformation at the thermodynamic limit	12
3.4.1	Thermodynamic properties	12
4	The antiferromagnetic case	15
4.1	Small number of spins	15
4.2	Thermodynamic limit	19
4.3	q -deformation for small number of spins	23
4.4	q -deformation of the thermodynamic limit	28
5	Conclusions	32

1 Introduction

The Kittel–Shore (KS) model [1] describes an infinite-range spin system in which N spins interact identically. It can be regarded as a vectorial extension of the Ising model: while Ising spins only possess a z -component, KS spins span the full $\mathfrak{su}(2)$ algebra. Because of this relationship, the KS Hamiltonian has been used in several Ising-based analyses, including the demonstration of the exactness of the molecular field approximation [1] and the study of first-order transitions in $J = 1$ Ising systems with crystal-field splitting [2]. Finite-size Ising simulations have also exploited KS results to infer higher-dimensional behaviour [3], and mappings of quantum spin partition functions to Ising models have been formulated through generalised Trotter product expansions [4, 5]. Further connections appear in studies of long-range quantum magnetism and quantum information [6, 7].

The exact solvability of the KS model follows from the decomposition of the tensor product of N irreducible $U(\mathfrak{su}(2))$ representations into invariant subspaces [1], making techniques such as the Bethe Ansatz unnecessary. It serves as a canonical and analytically tractable representative of long-range interacting spin models and exhibits a ferromagnetic phase transition that develops slowly as the system size increases [1]. These properties support finite-size scaling analyses in infinitely coordinated systems [8, 9], in accordance with Fisher’s and Barber’s scaling hypothesis [10]. Arbitrary spin extensions were developed in [6, 7, 11], and antiferromagnetic couplings were examined in [11, 12].

It is worth emphasising that the KS Hamiltonian corresponds to the Heisenberg XXX model on the complete graph [13], that is, the long-range generalisation of the XXX model with a fully symmetric constant coupling and thus a standard mean-field Hamiltonian [14] (once $I \rightarrow I/N$). Models on the complete graph exhibit strong analytical accessibility. In the spin-1/2 and spin-1 cases, integral formulas for the thermodynamic-limit partition function (ferromagnetic regime), explicit magnetisation, free energy, and critical exponents are available [6, 13, 15–20]. In the spin-1 setting, KS-type Hamiltonians have also been studied as bilinear–biquadratic models [21, 22]. Rotational and permutational symmetries are fundamental in deriving most of these results.

Geometrically, the KS Hamiltonian (H_{KS}) describes N spins at the vertices of a $(N - 1)$ -dimensional simplex, becoming effectively infinite dimensional in the thermodynamic limit $N \rightarrow \infty$. Small systems with $N = 2, 3, 4$ have been used to model ultra-small magnetic clusters [23] and appear in quantum-dot-based quantum computation proposals [24, 25].

The classical KS model was analysed in terms of the dynamics and integrals of motion. Its time evolution was studied in [26], invariants and action-angle variables were obtained in [27], and analytical autocorrelation functions were derived in [28]. Anisotropic generalisations (equivalent-neighbour XYZ) and their correlation functions were addressed in [29, 30].

Quantum groups, such as $U_q(\mathfrak{su}(2))$, underlie the symmetries of integrable spin chains like the XXZ Heisenberg model for N spin- $\frac{1}{2}$ particles, with the deformation parameter q linked to the anisotropy δ by $\delta = (q + q^{-1})/2$ and an additional boundary term $(q - q^{-1})(\sigma_z^1 - \sigma_z^N)/2$ [31–35]. The XXZ chain represents a q -deformation of the isotropic XXX model, recovered as $q \rightarrow 1$, and retains $U_q(\mathfrak{su}(2))$ -invariance in its conserved quantities [36]. Various other long-range interacting models with $U_q(\mathfrak{su}(2))$ symmetry exist, including the braid-translated q -deformed periodic XXZ chain [37, 38], the q -deformed Haldane–Shastry model [39], and systems with quantum affine algebra symmetry [40]. Elliptic extensions and integrable deformations have also been constructed [41, 42]. These q -deformed models typically exhibit nonlocal interactions, which is a feature shared by the model introduced here.

More generally, the Hopf algebra formalism [43] and the $\mathfrak{su}_q(2)$ deformation [44, 45] have led to numerous physical applications, including deformed bosons in pairing correlations [46], perturbative studies of the Dicke model [47], the q -rotator in diatomic molecular spectroscopy [48], thermodynamic properties of deformed fermionic systems [49, 50], and stability analyses comparing $\mathfrak{su}(2)$ and $\mathfrak{su}_q(2)$ symmetric systems [51]. This approach also permits analytical solutions, as in models where bosonic interactions can be embedded via an appropriate q -deformation of the $\mathfrak{su}(2)$ fermionic algebra [52].

In this work, we consider the q -deformation of the KS model introduced in [53]. This is an integrable model that depends on the deformation parameter q with the underlying $\mathfrak{su}_q(2)$ symmetry. The Curie temperature was obtained in [53] for the deformed case, but the thermodynamic properties of this deformed model were not discussed. This is the aim of this paper. In particular, we will focus on the specific heat, magnetic susceptibility, and magnetization when the angular momentum of the individual spins is $j = 1/2$, for both the antiferromagnetic and ferromagnetic scenarios. The deformation parameter modifies the energy spectrum by increasing the spacing between the energy

levels, thereby shifting the thermodynamic behaviour toward higher temperatures. In the ferromagnetic case, the deformation shifts the Curie temperature to higher values and narrows the specific heat peaks, whereas in the antiferromagnetic case, analytical approximations based on the two most probable energy levels accurately describe the thermodynamic quantities and the phase transitions. Overall, deformation introduces non-identical spin couplings, which significantly influence the thermodynamic behaviour compared to that of the undeformed KS model.

The structure of this paper is organized as follows. In Sec. 2, the Kittel-Shore model and its deformation based on $\mathfrak{su}_q(2)$ symmetry are presented. Then, in Sec. 3, we analyse the thermodynamic properties in the undeformed and deformed scenarios for the ferromagnetic case, whereas Sec. 4 focuses on the antiferromagnetic case. Finally, Sec. 5 presents our conclusions, highlighting the potential applications of this deformed model and directions for future research.

2 The Kittel–Shore model and its q -deformation

We present the KS model [1] for a system of N spins with an external magnetic field, but we start from the expression given in [11] (a difference of a factor of 2), making it easier to compare that paper and our results. This Hamiltonian reads

$$H_{KS} = -I \sum_{i < j}^N \vec{J}_i \cdot \vec{J}_j - \gamma h \sum_{i=1}^N J_z^{(i)}, \quad (1)$$

where I is the interaction constant between the spins, $\gamma = g\mu_B$ in the usual notation, and h is the external magnetic field. The interaction constant distinguishes between antiferromagnetic and ferromagnetic cases depending on its sign (negative or positive, respectively).

By definition, the angular momenta operators are given by

$$J_x = \frac{1}{2} \sigma_x, \quad J_y = \frac{1}{2} \sigma_y, \quad J_z = \frac{1}{2} \sigma_z, \quad (2)$$

being σ_i the Pauli matrices

$$\sigma_x = \begin{pmatrix} 0 & 1 \\ 1 & 0 \end{pmatrix}, \quad \sigma_y = \begin{pmatrix} 0 & -i \\ i & 0 \end{pmatrix}, \quad \sigma_z = \begin{pmatrix} 1 & 0 \\ 0 & -1 \end{pmatrix}. \quad (3)$$

With the definition of angular momentum operators given in (2), we can write

$$J_{\pm} = J_x \pm i J_y, \quad (4)$$

and, therefore

$$J_x = \frac{1}{2}(J_+ + J_-), \quad J_y = -\frac{i}{2}(J_+ - J_-), \quad (5)$$

so the matrix form of the $\{J_+, J_-, J_z\}$ operators are given by

$$J_+ = \begin{pmatrix} 0 & 1 \\ 0 & 0 \end{pmatrix}, \quad J_- = \begin{pmatrix} 0 & 0 \\ 1 & 0 \end{pmatrix}, \quad J_z = \frac{1}{2} \begin{pmatrix} 1 & 0 \\ 0 & -1 \end{pmatrix}. \quad (6)$$

Then, the Hamiltonian of Eq. (1) can be written as [53]

$$\tilde{H}_{KS} = -\frac{I}{2} \left(\sum_{i=1}^N J_-^{(i)} J_+^{(i)} + \sum_{i=1}^{N-1} \sum_{r=i+1}^N (J_-^{(i)} J_+^{(r)} + J_+^{(i)} J_-^{(r)}) + \left[\sum_{i=1}^N J_z^{(i)} \right]_q \left[\sum_{s=1}^N J_z^{(s)} + \mathbf{I}^{(N)} \right]_q - \sum_{i=1}^N C^{(i)} \right) - \gamma h \sum_{i=1}^N J_z^{(i)}, \quad (7)$$

where $C^{(i)}$ is the Casimir of the $\mathfrak{su}(2)$ algebra, given by

$$C^{(i)} = J_-^{(i)} J_+^{(i)} + J_z^{(i)} (J_z^{(i)} + 1) = J_+^{(i)} J_-^{(i)} + J_z^{(i)} (J_z^{(i)} - 1). \quad (8)$$

Consequently, the eigenvalues of the Hamiltonian (7) for a spin chain consisting of particles with identical spin j are

$$E_{NJm} = -\frac{I}{2} (J(J+1) - Nj(j+1)) - \gamma hm, \quad (9)$$

where $J = \sum_{i=1}^N j = Nj$ and $m = \sum_{i=1}^N m_i$, being m_i is the eigenvalue of the operator J_i^z . This implies that the eigenvectors of the Hamiltonian (7) are those given by the Clebsch–Gordan coefficients.

The Hamiltonian (7) can be deformed owing to its coalgebra symmetry [54]. Then, a new superintegrable model (maximally superintegrable for vanishing external magnetic field) is obtained when deforming this Hamiltonian through $U_q(\mathfrak{su}(2))$, which reads [53]

$$\begin{aligned} \tilde{H}_{KS}^q = & -\frac{I}{2} \left(\sum_{i=1}^N \exp \left[-\eta \sum_{j=1}^{i-1} J_z^{(j)} \right] J_-^{(i)} J_+^{(i)} \exp \left[\eta \sum_{h=i+1}^N J_z^{(h)} \right] + \sum_{i=1}^{N-1} \sum_{r=i+1}^N \left(e^{\eta/2} J_-^{(i)} J_+^{(r)} + e^{-\eta/2} J_+^{(i)} J_-^{(r)} \right) \right. \\ & \cdot \exp \left[-\eta \frac{J_z^{(i)}}{2} \right] \cdot \exp \left[\eta \frac{J_z^{(r)}}{2} \right] \cdot \prod_{t=1}^{i-1} \exp \left[-\eta J_z^{(t)} \right] \prod_{k=r+1}^N \exp \left[\eta J_z^{(k)} \right] + \left[\sum_{i=1}^N J_z^{(i)} \right]_q \left[\sum_{s=1}^N J_z^{(s)} + \mathbf{I}^{(N)} \right]_q - \\ & \left. - \sum_{i=1}^N C_q^{(i)} \right) - \gamma h \sum_{i=1}^N J_z^{(i)}, \end{aligned} \quad (10)$$

where $q = e^\eta$, $C_q^{(i)}$ is the Casimir operator for the algebra $\mathfrak{su}_q(2)$

$$C_q^{(i)} = J_-^{(i)} J_+^{(i)} + [J_z^{(i)}]_q [J_z^{(i)} + \mathbf{I}]_q = J_+^{(i)} J_-^{(i)} + [J_z^{(i)}]_q [J_z^{(i)} - \mathbf{I}]_q, \quad (11)$$

and

$$[n]_q := \frac{q^{n/2} - q^{-n/2}}{q^{1/2} - q^{-1/2}}. \quad (12)$$

Then, for $q = 1$ (equivalently, $\eta = 0$), the deformed Hamiltonian (10) leads to the undeformed KS Hamiltonian (7). For the particular case of 1/2-spin particles, the angular momentum operators of the algebra $\mathfrak{su}_q(2)$ are those in Eq. (6), that is, independent of the parameter q [44].

Following the rules of action of angular momentum operators, it is easy to obtain that the corresponding eigenvalues of this deformed Hamiltonian are

$$E_{NJm}^q = -\frac{I}{2} ([J]_q [J+1]_q - N[j]_q [j+1]_q) - \gamma hm. \quad (13)$$

The energy distribution of the deformed model reveals that deformation increases the spacing between the energy levels [53]. This dilation of the differences between levels is more prominent for those with a larger J .

The distribution of energy levels in the undeformed ferromagnetic and antiferromagnetic cases was studied in [12, 53]. In the ferromagnetic case, the ground energy states are the most separated energy levels and have the lowest degree of degeneracy. In contrast, the lowest energy levels are very close in the antiferromagnetic case. This allows the energy distribution to be considered as a continuum in this range. Moreover, the antiferromagnetic degeneracy is larger in the low-energy range. These phenomena are mainly responsible for the fact that we can use good (approximate) analytical approaches for the antiferromagnetic case but not for the ferromagnetic case, as discussed in the following sections.

Once the Hamiltonian is given, the partition function for the N -spins problem can be obtained from

$$Z_N = \sum_J \sum_{m=-J}^{m=J} d_{NJ} \exp(-\beta E_{NJm}), \quad (14)$$

where $\beta = 1/k_B T$ and the coefficients d_{NJ} represent the multiplicity of the state of N spins with total angular momentum J and quantum number m . These coefficients are given by [55]

$$d_{NJ} = \Omega(N, J) - \Omega(N, J+1), \quad \text{with} \quad \Omega(N, J) = \text{coefficient of } x^J \text{ in } (x^j + x^{j-1} + \cdots + x^{-j})^N. \quad (15)$$

For the particular case considered in this work, $j = 1/2$, the previous expression can be written as [11]

$$d_{NJ} = \binom{N}{N/2 - J} - \binom{N}{N/2 - (J+1)}. \quad (16)$$

For the deformed case, we will use

$$Z_N^q = \sum_J \sum_{m_J=-J}^{m_J=+J} d_{NJ} \exp(-\beta E_{NJm}^q), \quad (17)$$

Notably, the degeneracies of this model are not modified when deformation is applied.

This partition function can be used to obtain the Helmholtz free energy, $F = -(k_B T/N) \log(Z)$. All thermodynamic functions can be obtained by differentiating this energy. The specific heat, magnetic susceptibility, and magnetisation are given by

$$C_V = -T \frac{\partial^2 F}{\partial T^2} \Big|_{h=0}, \quad \chi = - \frac{\partial^2 F}{\partial H^2} \Big|_{h=0}, \quad M = -\frac{\partial F}{\partial H}. \quad (18)$$

In the following, we study these properties for antiferromagnets and ferromagnets corresponding to $I = -1$ and $I = 1$, respectively.

3 The ferromagnetic case

We begin with the ferromagnetic case and discuss the KS model for a small number of spins and for the thermodynamic limit.

3.1 Small number of spins

Using the expressions in Eq. (18), the thermodynamic properties of the undeformed model are represented. As illustrated in Fig. 1, the specific heat exhibits a higher maximum value and is shifted to the right for larger values of N . Moreover, we observe the same behaviour regardless of whether N is odd or even.

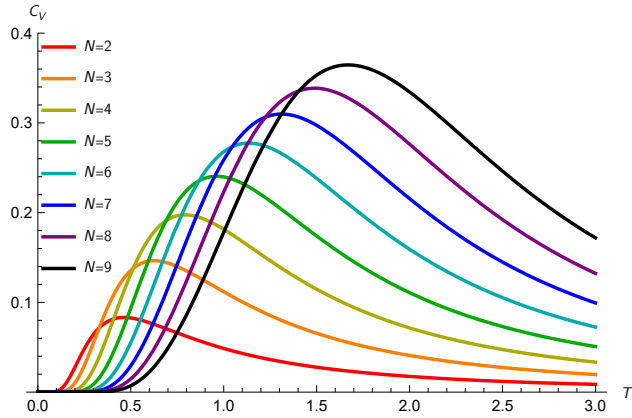


Figure 1: Specific heat as a function of temperature for values of the number of particles $N = 2$ (red), 3 (orange), 4 (yellow), 5 (green), 6 (cyan), 7 (blue), 8 (purple), and 9 (black) for the ferromagnetic case.

We can now try to understand why the specific heat shows this behaviour, in particular, why it increases and its maximum is shifted to higher temperatures as N increases. The density of the energy levels is considerably separated

in the ferromagnetic case; therefore, its energy profile is discrete throughout the range considered [12]. Moreover, it can be seen that an important contribution to the peak is due to the two most probable levels (the lower the number of particles, the greater the contribution). Therefore, these temperatures are approximately proportional to the difference between the fundamental and first excited energy levels, $T \propto \Delta E$. A simple calculation using Eq. (9) yields $E_1 - E_0 = IN/2$, which means $T \propto N$. This fact explains why the model cannot be applied to a large number of particles in the ferromagnetic case, as extremely high temperatures are required to be considered a realistic model. Therefore, the ferromagnetic model for more than nine spins was not analysed. Later in this section, we will consider the thermodynamic limit in which a large number of spins are considered, but the interaction constant I is replaced by I/N , so the aforementioned behaviour is not present, and it can then be completely analysed.

For magnetic susceptibility, one can observe a behaviour $1/(NT)$, independent of the parity of N , as shown in Fig. 2.

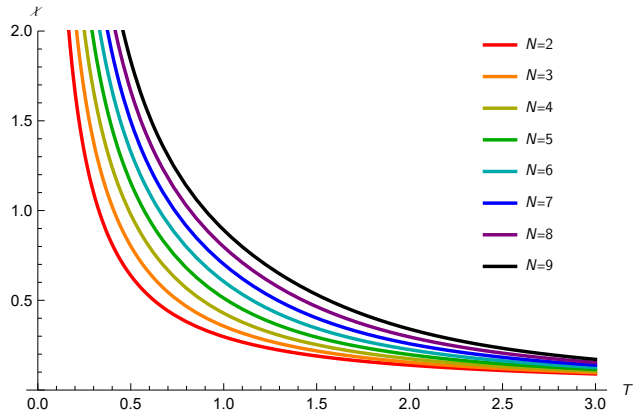


Figure 2: Magnetic susceptibility as a function of temperature for values of the number of particles $N = 2$ (red), 3 (orange), 4 (yellow), 5 (green), 6 (cyan), 7 (blue), 8 (purple), and 9 (black) for the ferromagnetic case.

Finally, the magnetisation is shown in Fig. 3 for an external magnetic field (in $h = \gamma = 1$ units). We observe that at zero temperature, the magnetisation is $1/2$, which is independent of the number of spins. Because all spins point in the same direction in this case, the magnetisation is given by $M = m/N = Nj/N = 1/2$. At higher temperatures, the spins become more delineated, and the magnetisation becomes zero.

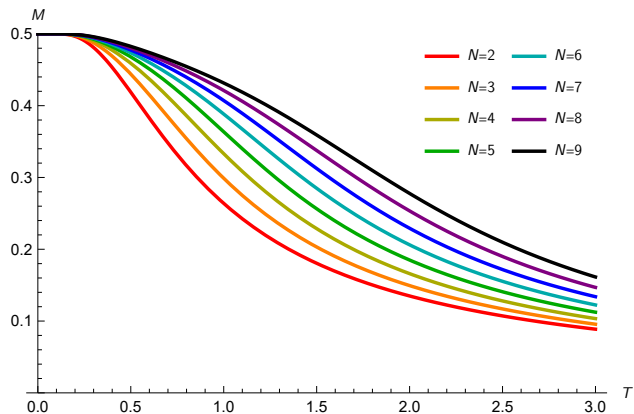


Figure 3: Magnetisation as a function of temperature for values of the number of particles $N = 2$ (red), 3 (orange), 4 (yellow), 5 (green), 6 (cyan), 7 (blue), 8 (purple), and 9 (black), with $h = \gamma = 1$ for the ferromagnetic case.

We also find a critical change of the magnetisation at $h = 0$ for the temperature $T = 0^+$ obtained in [56], as shown in Fig. 4.

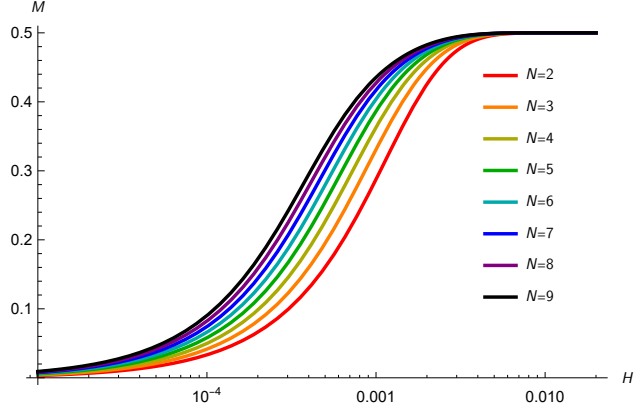


Figure 4: Magnetisation as a function of magnetic field for values of the number of particles $N = 2$ (red), 3 (orange), 4 (yellow), 5 (green), 6 (cyan), 7 (blue), 8 (purple), and 9 (black) for temperature $T = 0^+$, for the ferromagnetic case.

The chosen temperature is $T = 0.001$ and the closer this value is to 0, the sharper are the represented curves. The least energetic state for $h = 0$ is shared by all configurations with the largest value J . Therefore, the average magnetisation of the set of configurations is zero. When a small magnetic field is applied, this degeneracy is broken, and the least energetic state is given by all spins up with the largest J . Thus, the magnetisation reaches its maximum value at this point and does not decrease again because as the magnetic field increases, the previous state becomes less energetic. This occurs for N being even and odd.

3.2 Thermodynamic limit

To consider the thermodynamic limit, we change $I \rightarrow I/N$, allowing the thermodynamic properties to be accurately described [12].

3.2.1 Thermodynamic properties

Now, the behaviour of the thermodynamic properties are examined in the thermodynamic limit. The numbers of particles $N = 100, 500$ and 1000 are selected because parity does not play a significant role in the ferromagnetic case. This is due to the fact that, unlike in the antiferromagnetic case, where the ground state depends on the parity of N (as we will see in the following section), the ferromagnetic ground states ($J = N/2, N/2 - 1$) remain unchanged.

The three properties analysed here diverge or show peaks near the Curie temperature ($T_C = 0.25$ [1]), indicating a phase transition [57]. In Fig. 5, we observe that the specific heat peaks occur at nearly the same temperature and become slightly larger as the number of particles increases, showing the transition.

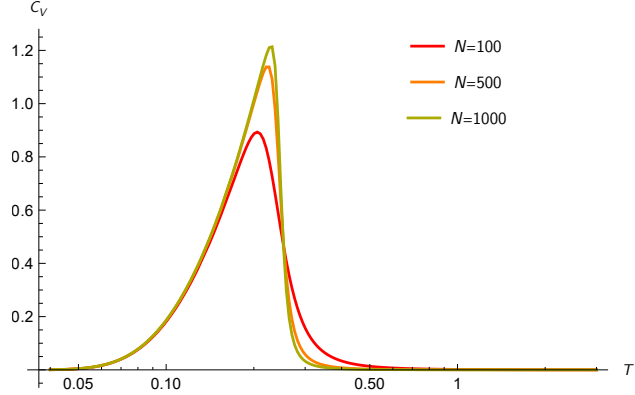


Figure 5: Specific heat as a function of temperature for values of the number of particles $N = 100$ (red), 500 (orange), and 1000 (yellow), for the interaction constant $I = 1/N$ ferromagnetic case.

In Fig. 6, magnetic susceptibility exhibits convergence at both low temperatures, where it diverges to infinity, and at high temperatures, where it approaches zero. In the intermediate range, the curve shows a Curie transition, which will be discussed later. The curves differ only during this transition, which occurs at almost the same temperature but reaches higher susceptibility values as the number of particles increases.

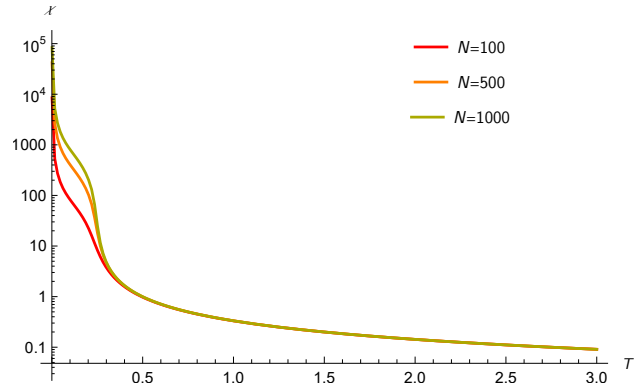


Figure 6: Magnetic susceptibility as a function of temperature for values of the number of particles $N = 100$ (red), 500 (orange), and 1000 (yellow), for the interaction constant $I = 1/N$ ferromagnetic case.

In Fig. 7, we present the magnetisation with and without an external magnetic field. This thermodynamic property is directly related to magnetic susceptibility; therefore, the one without an external magnetic field also allows one to observe the Curie transition. In the figure with an external magnetic field, we can see that all the N curves coincide in the thermodynamic limit, independently of the temperature.

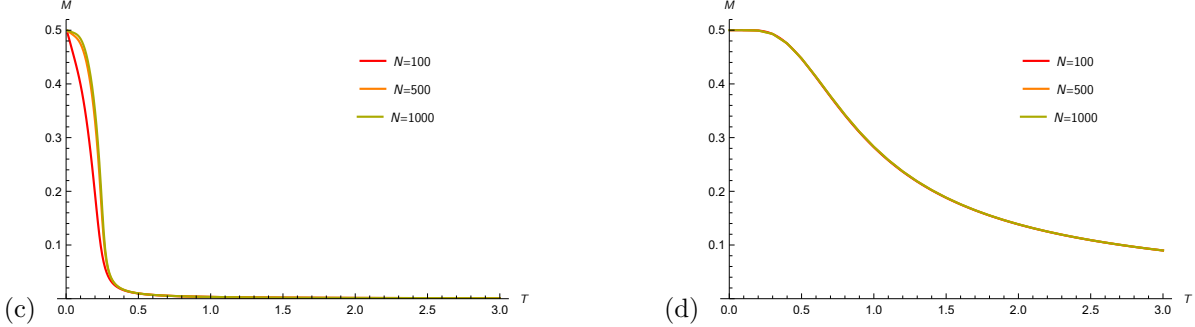


Figure 7: Magnetisation as a function of temperature for values of the number of particles $N = 100$ (red), 500 (orange), and 1000 (yellow), for the interaction constant $I = 1/N$ and (a) external magnetic field $h = \gamma = 0$, (b) $h = \gamma = 1$ ferromagnetic case. They all are coincident.

In the absence of an external magnetic field, we can observe from the thermodynamic properties that the Curie temperature is approximately the same for every number of particles, as discussed in [1]. When an external magnetic field is introduced, differences appear. The modification of the coupling and the presence of an external magnetic field cause the magnetic term in Eq. (9) to become dominant. Consequently, the most probable state remains $|N/2, N/2\rangle$, but the energy distribution undergoes significant changes because the energy differences are proportional to the external magnetic field h . Thus, the magnetisation takes the value $M = 0.5$ at $T = 0$ and decreases when the next energy level is reached. This decrease is practically the same for all curves because the energy levels depend on N , and the numbers chosen here are sufficiently large that the differences in magnetisation are minimal.

By the dominance of the magnetic part, it is possible to analytically obtain the expression of magnetisation in the thermodynamic limit using the approximation of the most probable levels ($J = N/2, N/2 - 1$):

$$M^{TL} = \frac{A - B + C + D}{E}, \quad (19)$$

where

$$\begin{aligned} A &= (N - 2)(N - 1)e^{1/T}, \\ B &= N(N - 1)e^{2/T}, \\ C &= Ne^{\frac{1}{2T}} - (N + 2)e^{\frac{3}{2T}}, \\ D &= e^{N/T} \left((N - 2)(N - 1) \left(-e^{1/T} \right) - Ne^{\frac{5}{2T}} + (N + 2)e^{\frac{3}{2T}} + N(N - 1) \right), \\ E &= 2N \left(e^{1/T} - 1 \right) \left((N - 1)e^{1/T} - e^{N/T} \left(N + e^{\frac{3}{2T}} - 1 \right) + e^{\frac{1}{2T}} \right). \end{aligned}$$

This expression does not accurately reproduce the magnetisation at temperatures above the Curie transition because the ground states are the least degenerate. However, it provides a highly precise approximation at low temperatures, particularly for identifying transition points. In the undeformed case, an exact analytical expression for the thermodynamic functions of the model, including the magnetisation, can be obtained without approximations, as shown in Ref. [7]. However, such a closed-form treatment is not feasible for the q -deformed Hamiltonian, so here we employ the most-probable-level approximation ($J = N/2, N/2 - 1$) in the thermodynamic limit to obtain an analytic expression that will serve as a reference for comparison with the deformed case.

3.3 q -deformation for small number of spins

We begin by considering the q -deformed model for a small number of spins. We can note that the modification due to the variation of the deformation parameter becomes more appreciable for q and N larger. This is due to the fact that the energy values depend on the number of particles and q -number properties, so that the modulus of the energy of many particles becomes greater than the one of a few particles when a deformation is introduced ($(|x| + 1)_q - (|x| + 1) > [|x|_q - |x|]$).

We begin with the specific heat shown in Fig. 8. It is important to note that the maxima remain with the same magnitude and are placed further to the right for increasing values of η , which follows the reasoning discussed above. Note that the negative values of the parameter η have not been plotted because the model is symmetric with respect to $\eta = 0$.

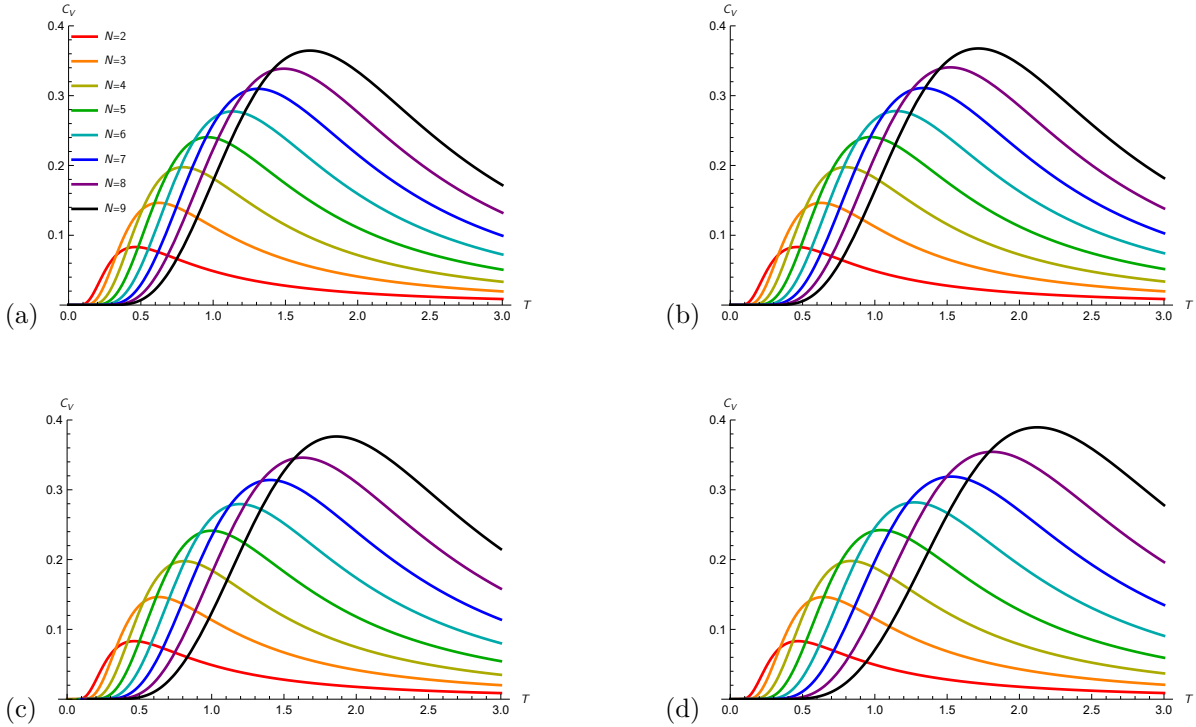
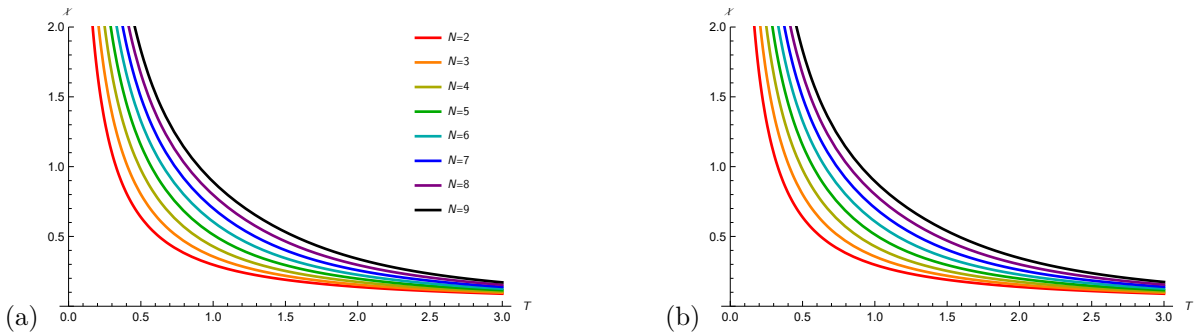


Figure 8: Specific heat as a function of temperature for values of the number of particles $N = 2$ (red), 3 (orange), 4 (yellow), 5 (green), 6 (cyan), 7 (blue), 8 (purple), and 9 (black) and of the parameter (a) $\eta = 0$, (b) $\eta = 0.1$, (c) $\eta = 0.2$, and (d) $\eta = 0.3$, for the ferromagnetic case.

As for the undeformed case, the temperature at which the maximum specific heat appears is proportional to the difference between the two fundamental levels, $T \propto E_1 - E_2$. Therefore, the maximum value of the deformation parameter considered was $\eta = 0.3$. Higher deformation parameters do not allow us to observe the peaks properly within the considered temperature range.

The magnetic susceptibility is shown in Fig. 9. We observe that while there are small differences between the plots depending on the value of η , the behaviour $1/(NT)$ is not modified at high temperatures.



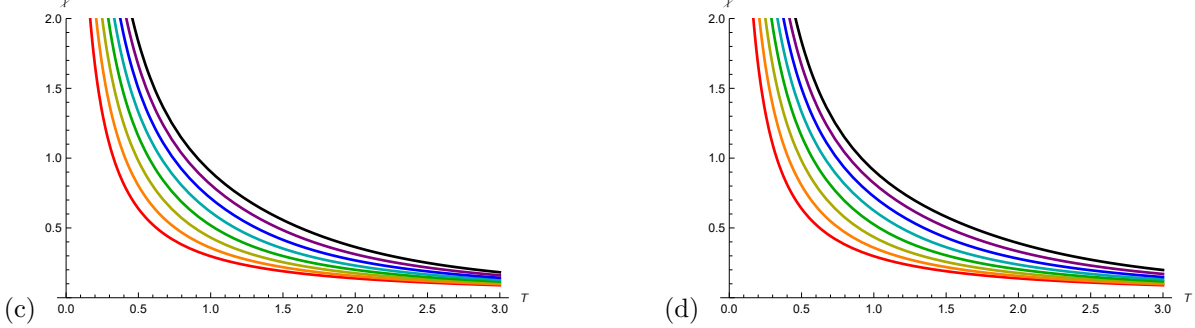


Figure 9: Magnetic susceptibility as a function of temperature for values of the number of particles $N = 2$ (red), 3 (orange), 4 (yellow), 5 (green), 6 (cyan), 7 (blue), 8 (purple), and 9 (black) and of the parameter (a) $\eta = 0$, (b) $\eta = 0.1$, (c) $\eta = 0.2$, and (d) $\eta = 0.3$, for the ferromagnetic case.

The magnetisation is shown in Fig. 10. Here, we do not find any difference between N odd or even, as in the undeformed case. The only modification with respect to the undeformed case is a small change in the convexity of the function for large N when η increases, because the q -deformation makes the energy levels become more separated, and therefore the interaction energy is greater with respect to the undeformed case.

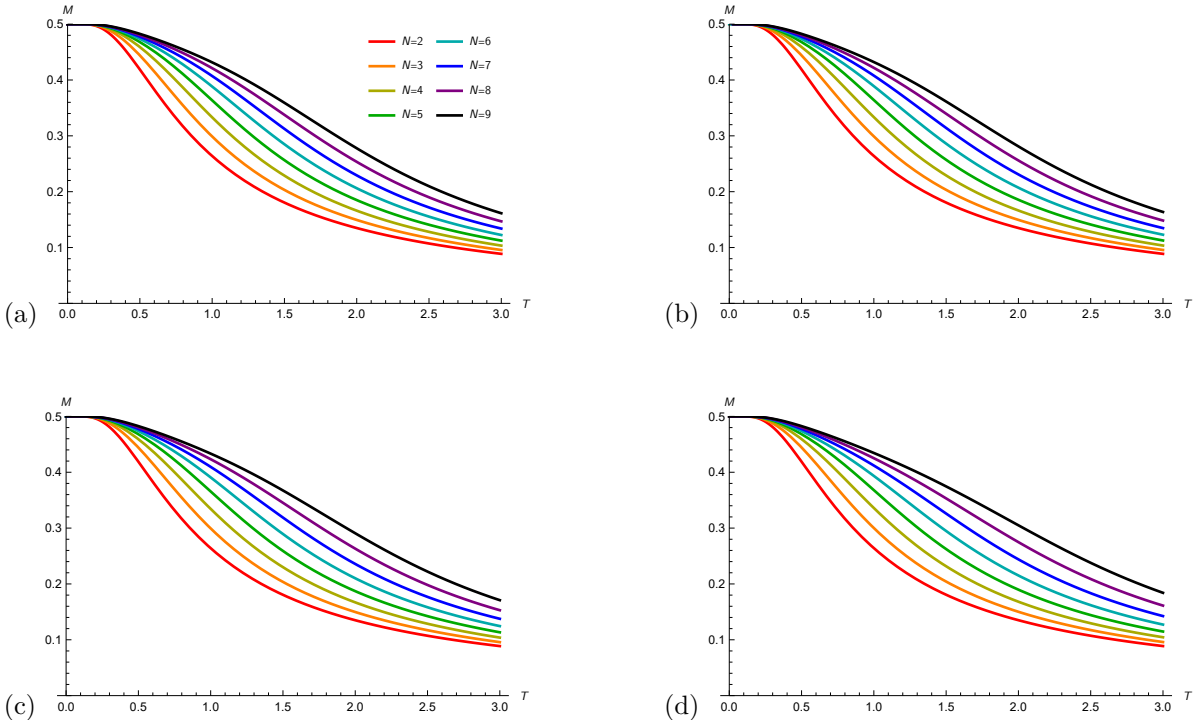


Figure 10: Magnetisation as a function of temperature for values of the number of particles $N = 2$ (red), 3 (orange), 4 (yellow), 5 (green), 6 (cyan), 7 (blue), 8 (purple), and 9 (black) and of the parameter (a) $\eta = 0$, (b) $\eta = 0.1$, (c) $\eta = 0.2$, and (d) $\eta = 0.3$, for the $h = \gamma = 1$ ferromagnetic case.

As in the undeformed case, we find a change in the magnetisation for $h = 0$ at $T = 0^+$, independent of the value of q ; therefore, the corresponding graphs for different values of q are not presented. Furthermore, at $h = 0$, the state with the lowest energy is shared by every possible configuration (each m) at the highest J level for any q , given a specific N , although this varies with the number of particles. This implies that the average magnetisation is zero. When a small magnetic field h is applied, the ground state is no longer shared by all states with the maximum J , but only by that for which $m = J$. Thus, the magnetisation reaches its maximum possible value and is maintained

for any value $h > 0$ and for any q deformation parameter. In fact, the larger the deformation, the less energetic the previous state is.

3.4 q -deformation at the thermodynamic limit

We now consider the thermodynamic limit in the deformed scenario. As stated in [53], the deformed energy eigenvalues are now given by q -numbers, which grow exponentially for large values of η . Therefore, the simplest form to assure the extensibility of the model for an arbitrary N consists of defining the coupling constant of the deformed model as $I \rightarrow I/N$ (as in the undeformed KS model) and the deformation parameter as $\eta \rightarrow \eta/N$. Thus, in the following thermodynamic limits, we consider the q -KS model with the deformation parameter $q = e^{\eta/N}$.

3.4.1 Thermodynamic properties

In the undeformed case, the thermodynamic properties exhibit a behaviour in which the number of particles has little to no influence. In contrast, in the deformed case, it has been observed that the curves corresponding to different particle numbers are significantly more separated (as we will see in Figs. 11, 12, 13, and 14). Moreover, this effect becomes more pronounced as the deformation increases.

The Curie temperature was obtained in [53]. For small and intermediate deformation parameters ($\eta \in (0, 8)$), it is approximated as (see [53] for the derivation and details of these results)

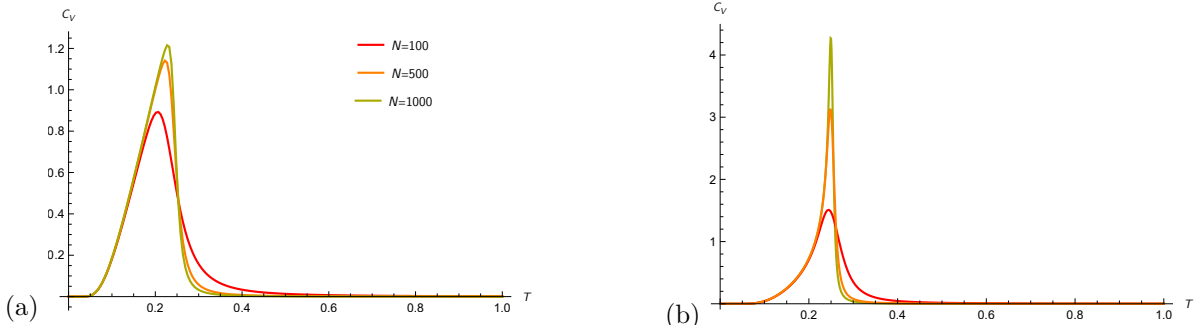
$$T_C(\eta) = 0.25 \quad \eta \in (0, 3), \quad (20)$$

$$T_C(\eta) = 0.25 + 0.022959\eta - 0.023077\eta^2 + 0.007164\eta^3 - 0.000779\eta^4 + 0.000035\eta^5 \quad \eta \in (3, 8), \quad (21)$$

while for larger values of η is

$$\lim_{N \rightarrow \infty} T_C(\eta) = \frac{e^{\eta/2}}{\eta^2 \log(4)}. \quad (22)$$

This temperature can be observed in the different thermodynamic magnitudes considered here, as we will see.



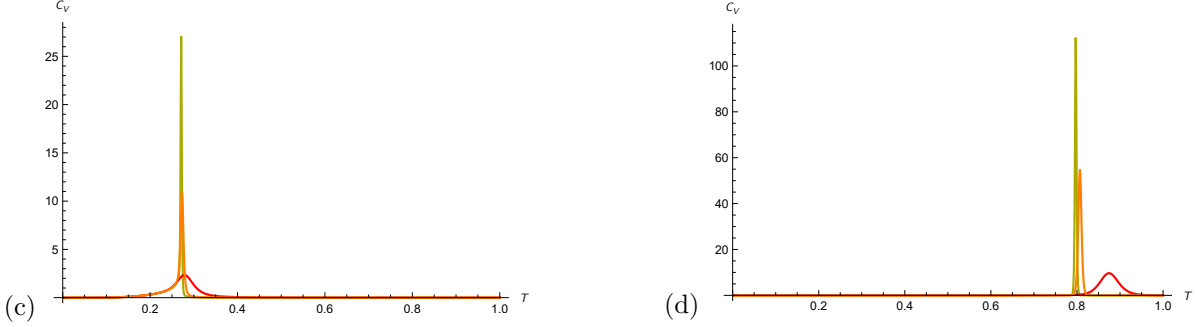


Figure 11: Specific heat as a function of temperature for values of the number of particles $N = 100$ (red), 500 (orange), and 1000 (yellow) for the interaction constant $I = 1/N$ ferromagnetic case. The values of the parameter $q = e^{\eta/N}$ are: (a) $\eta = 0$, (b) $\eta = 3$, (c) $\eta = 4$, and (d) $\eta = 9$.

For example, the peaks of the specific heat reach significantly higher values and occur at higher temperatures, although they also become narrower, as shown in Fig. 11. This behaviour arises because deformation broadens the energy distribution, reducing the influence of highly excited states and amplifying the action of the ground states within the considered temperature range.

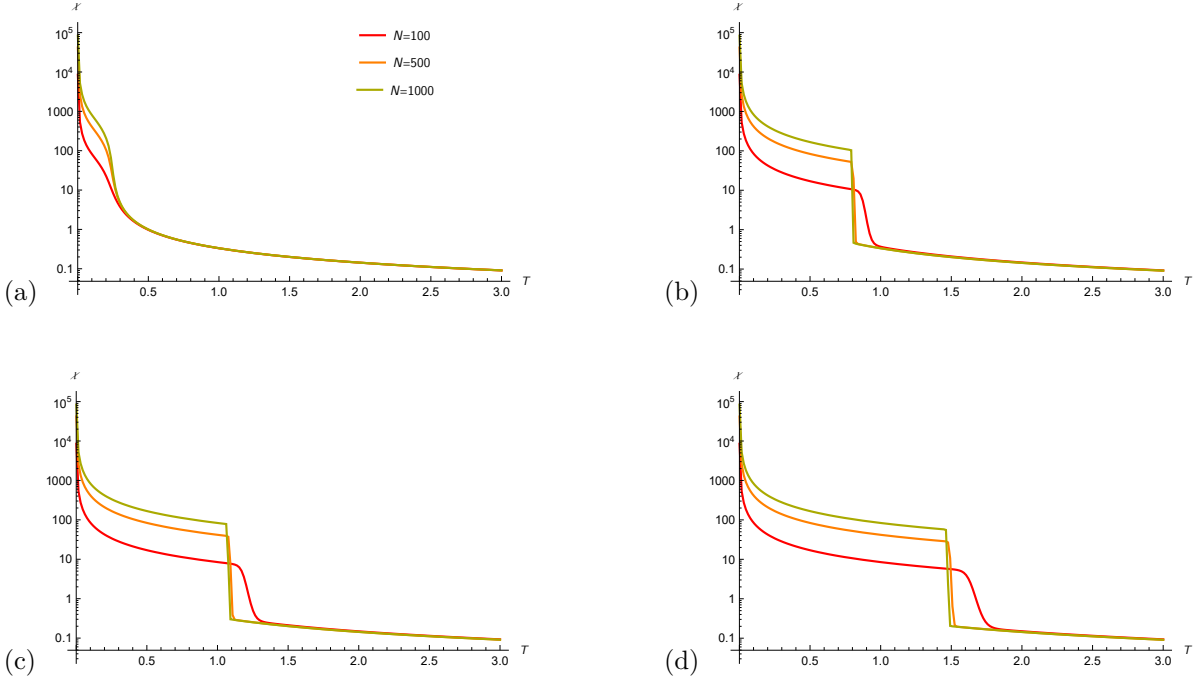


Figure 12: Magnetic susceptibility as a function of temperature for values of the number of particles $N = 100$ (red), 500 (orange), and 1000 (yellow) for the interaction constant $I = 1/N$ ferromagnetic case. The values of the parameter $q = e^{\eta/N}$ are: (a) $\eta = 0$, (b) $\eta = 9$, (c) $\eta = 10$, and (d) $\eta = 11$.

In terms of magnetic susceptibility, the introduction of deformation distorts the coincidence of the curves for different N observed in the undeformed case. This coincidence occurs for values before and after the Curie temperature, and the deformation shifts this convergence to lower and higher temperatures. This effect is amplified as the deformation parameter increases. As expected, the Curie transition occurs at progressively higher temperatures as the deformation increases. It can be observed that the transition temperature values in the susceptibility coincide with the temperature of the peaks in the specific heat for the same values of deformation and particle number, as expected. Regarding its shape, it becomes progressively less smooth, with the curve appearing increasingly more vertical as the deformation increases.

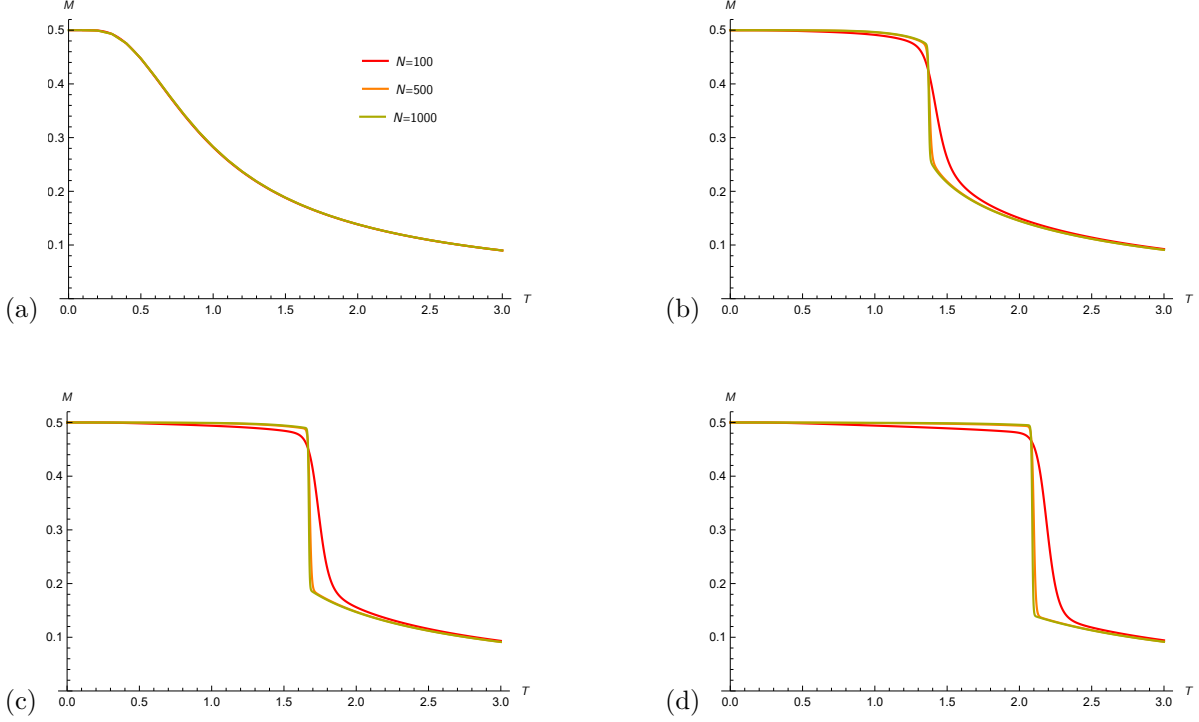
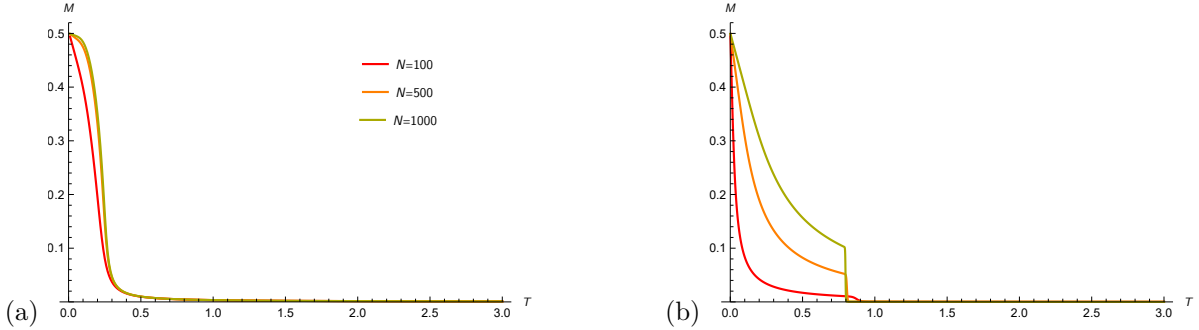


Figure 13: Magnetisation as a function of temperature for values of the number of particles $N = 100$ (red), 500 (orange), and 1000 (yellow) for the interaction constant $I = 1/N$ and $h = \gamma = 1$ ferromagnetic case. The values of the parameter $q = e^{\eta/N}$ are: (a) $\eta = 0$, (b) $\eta = 9$, (c) $\eta = 10$, and (d) $\eta = 11$.

In the undeformed case, all the magnetisation curves almost coincide, but they do not in the deformed case. Because the ground states remain the same in the deformed case (for a given N), a similar behaviour is observed at low temperatures for each deformation value. These four previous figures take an external magnetic field of $h = 1$, so we cannot see the Curie transition. Therefore, we reproduce these figures for a null external magnetic field.



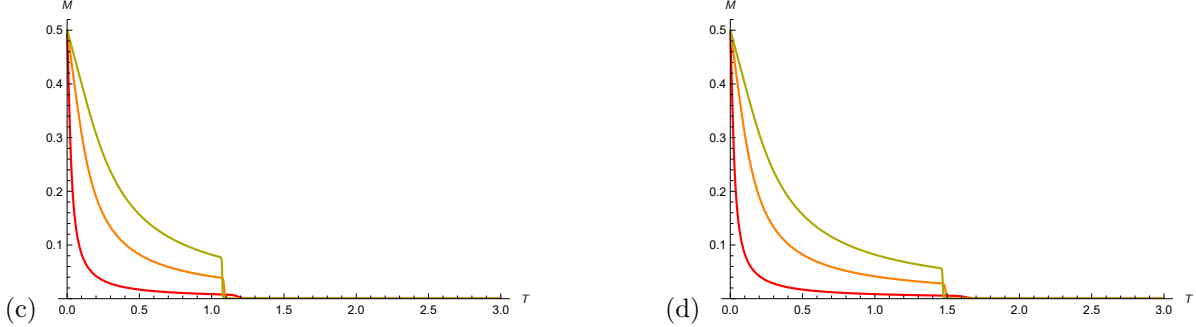


Figure 14: Magnetisation as a function of temperature for values of the number of particles $N = 100$ (red), 500 (orange), and 1000 (yellow) for the interaction constant $I = 1/N$ and $h = \gamma = 0$ ferromagnetic case. The values of the parameter $q = e^{\eta/N}$ are: (a) $\eta = 0$, (b) $\eta = 9$, (c) $\eta = 10$, and (d) $\eta = 11$.

We observe spontaneous magnetisation in the absence of an external magnetic field. As the temperature increases, the magnetisation gradually decreases until it reaches the Curie transition, at which a sharp drop occurs, ultimately reducing the magnetisation to zero.

4 The antiferromagnetic case

We now move to the antiferromagnetic case for both undeformed and deformed Hamiltonians, and for a small number of spins and its thermodynamic limit.

4.1 Small number of spins

We start by reproducing the results of [11] and extend them by computing the magnetisation and studying the corresponding behaviour at zero temperature. Using Eqs. (18), the graphs in that article corresponding to the specific heat can be easily reproduced, as shown in Fig. 15.

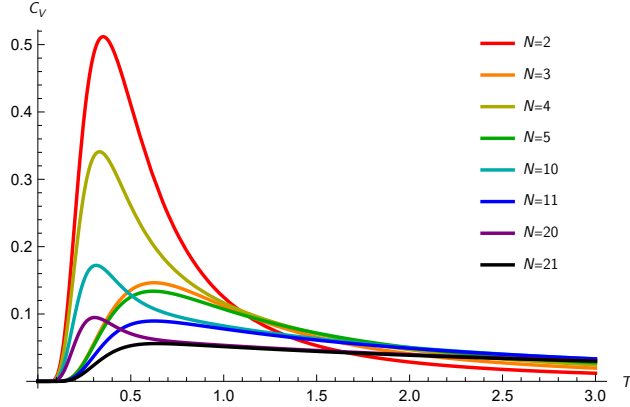


Figure 15: Specific heat as a function of temperature for values of the number of particles $N = 2$ (red), 3 (orange), 4 (yellow), 5 (green), 10 (cyan), 11 (blue), 20 (purple), and 21 (black) for the antiferromagnetic case.

We observe a completely different behaviour if N is odd or even. In the antiferromagnetic case, the ground states depend on the parity of the number of particles: for an even number of particles, they correspond to $J = 0, 1$, whereas for an odd number, they correspond to $J = 1/2, 3/2$. For N even, the maximum is shifted to the left as N increases. The position of this maximum depends mostly on the distance between the two lowest energy levels and, to a lesser extent, on the rate of degeneration of the two levels. This difference is I for N even and $3I/2$

for N odd, which quantifies the distance between the corresponding maxima. At high temperatures, a behaviour $1/T^2$ is observed as long as the number of particles is small (see the analytical expression of Eq. (24)) because the amplitude of the energy levels is proportional to N^2 ; therefore, the temperature range considered here does not allow the system to reach the highest energy levels when N increases [11].

For the magnetic susceptibility, we observe in Fig. 16 also a significant difference between even and odd N . This behaviour can be understood as follows. For odd N , the lowest energy level always splits into two in the presence of the magnetic field, whereas for even N it does not. In the odd- N case, one can have configurations with as many spins up as down except for a single spin, so that the local field produced by the remaining spins on that spin vanishes (frustration) and only the external field acts on it, as discussed in Ref. [11]. Moreover, for N odd, we observe a behaviour of $1/(NT)$, while in both cases, the behaviour decreases as $1/T$ at high temperatures (see the analytical expression of Eq. (25)).

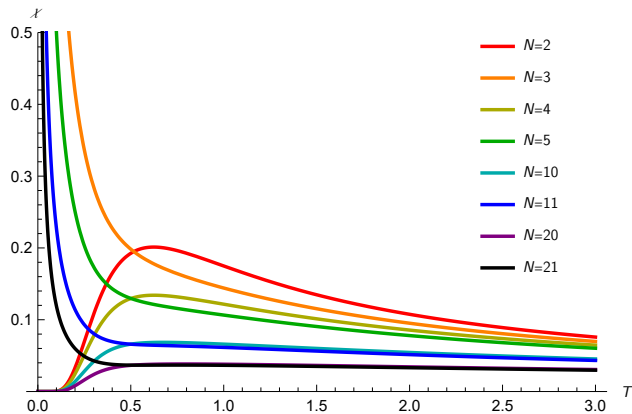


Figure 16: Magnetic susceptibility as a function of temperature for values of the number of particles $N = 2$ (red), 3 (orange), 4 (yellow), 5 (green), 10 (cyan), 11 (blue), 20 (purple), and 21 (black) for the antiferromagnetic case.

The magnetisation is shown in Fig. 17, for an external magnetic field (in $h = \gamma = 1$ units). In this scenario, we notice a slight bump at low temperatures when N is odd, whereas no such bump appears when N is even. Moreover, in both cases, it goes to zero for increasing N and T . As before, the main contribution to the magnetisation is from the two lower bands.

The fact that at $T \rightarrow 0$ there is a maximum for N even while there is a small bump for greater values of T for N odd can be understood from the following argument. For simplicity, we consider the cases $N = 2$ and $N = 3$. In the first case, the minimum energy is obtained for two different configurations: one spin up and one spin down, located in the $j = m = 0$ state (with energy $-3/4$), and both spins up, on the $j = m = 1$ (with energy $1/4 - h$). Therefore, the magnetisation at zero temperature is maximum, corresponding to the average of the last two configurations. When the temperature increases, the other configurations come into play; therefore, the magnetisation decreases, going to zero for a sufficiently high temperature (the average of the magnetisation for all the possible configurations is zero).

For the $N = 3$ case, the minimum energy configuration corresponds to the (doubly degenerate) $J = m = 1/2$ state (with energy $-3/4 - h/2$), with two spins up and one spin down. The first excited energy state corresponds to the three-spin-up configuration with $J = m = 3/2$ (with energy $3/4 - 3h/2$). Therefore, when the temperature increases slightly, the magnetisation slightly increases because the latter is in play, with the magnetisation being an average of these two states. This explains the small bump in the magnetisation for N odd. As in the N even case, the magnetisation for high temperatures goes to zero because the other configurations are also possible.

Following this argument, one can understand the behaviour for N even or odd for a larger number of spins.

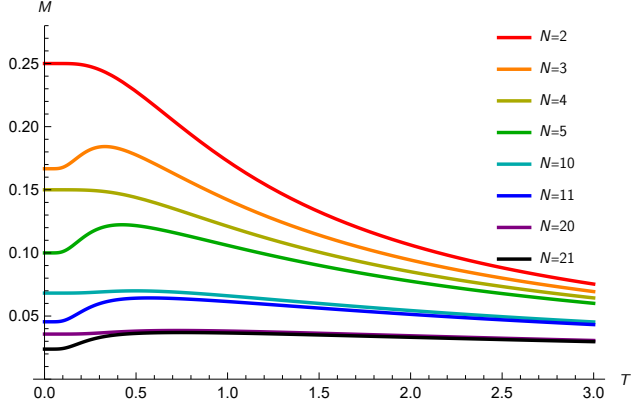


Figure 17: Magnetisation as a function of temperature for values of the number of particles $N = 2$ (red), 3 (orange), 4 (yellow), 5 (green), 10 (cyan), 11 (blue), 20 (purple), and 21 (black), with $h = \gamma = 1$ for antiferromagnetic case.

The behaviour of these three quantities, and in particular the fact that the lower energy levels play a prominent role, can be understood from the energy spectrum (9). One can notice that the most probable levels, those with the lowest energy, are those with the smallest J .¹ Therefore, for even N the greatest contribution is given by the levels with $J = 0, 1$, and for odd N the ones with $J = 1/2, 3/2$. For increasing N , the dominant term in the energy (9) becomes the one proportional to N . This allows us to consider an approximation of the partition function, for which the only terms that are considered are these, finding

$$Z^e = e^{-\frac{8h-3N+8}{8T}} \left(\left(\frac{N}{\frac{N}{2}}\right) e^{\frac{h+1}{T}} - \left(\frac{N}{\frac{N}{2}-2}\right) \left(e^{h/T} + e^{\frac{2h}{T}} + 1\right) + \left(\frac{N}{\frac{N}{2}-1}\right) \left(e^{h/T} + e^{\frac{2h}{T}} - e^{\frac{h+1}{T}} + 1\right) \right),$$

$$Z^o = \left(e^{h/T} + 1\right) \left(-e^{\frac{3(-4h+N-5)}{8T}}\right) \left(\left(\frac{N}{\frac{N-5}{2}}\right) \left(e^{\frac{2h}{T}} + 1\right) + \left(\frac{N}{\frac{N-3}{2}}\right) \left(-e^{\frac{2h}{T}} + e^{\frac{2h+3}{2T}} - 1\right) - \left(\frac{N}{\frac{N-1}{2}}\right) e^{\frac{2h+3}{2T}} \right). \quad (23)$$

Therefore, we can obtain analytical (and functional) expressions. In particular, we obtain the following for the specific heat:

$$C_V^e = \frac{9(N+4)e^{1/T}}{(9NT + (N+4)e^{1/T}T)^2}, \quad C_V^o = \frac{9(N-1)(N+5)e^{\frac{3}{2T}}}{NT^2 \left((N+5)e^{\frac{3}{2T}} + 4(N-1)\right)^2}, \quad (24)$$

where the superscripts e and o correspond to the even and odd N cases, respectively. The magnetic susceptibility reads

$$\chi^e = \frac{6}{9NT + (N+4)e^{1/T}T}, \quad \chi^o = \frac{(N+5)e^{\frac{3}{2T}} + 20(N-1)}{4NT \left((N+5)e^{\frac{3}{2T}} + 4(N-1)\right)}, \quad (25)$$

and finally, the magnetisation is

$$M^e = \frac{3(e^{2/T} - 1)}{3Ne^{1/T} + 4(N+1)e^{2/T} + 3N}, \quad M^o = \frac{(N-1)(e^{1/T} - 1)(e^{1/T}(3e^{1/T} + 4) + 3) + (N+5)e^{3/T} \sinh\left(\frac{1}{2T}\right)}{N(e^{1/T} + 1)(2(N-1)e^{2/T} + (N+5)e^{\frac{5}{2T}} + 2(N-1))}. \quad (26)$$

Before proceeding, we compare the approximation carried out by considering the two most probable levels and the results obtained when the entire partition function is considered. To determine the goodness of this approximation, the three thermodynamic properties considered above have been plotted, distinguishing between N even and odd cases. This is shown in Figs. 18-20.

¹It is important to note that states are defined just by angular momentum J when an external magnetic field is not applied. This holds for the specific heat and magnetic susceptibility, but not for magnetisation. The states are described by the angular momentum J and magnetic angular momentum m . The approximation we consider here takes only the J values (no the m ones) of the two most probable levels, so we always refer to it as the approximation of the most probable levels, since more than two states (due to the m degeneration) are indeed considered.

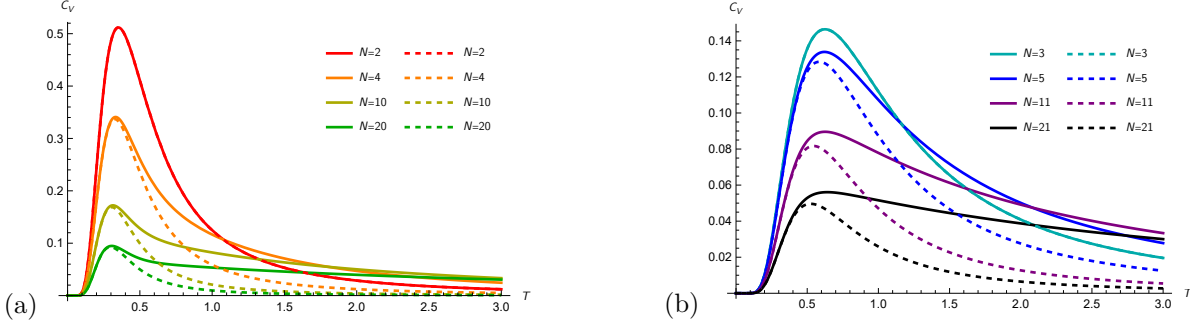


Figure 18: Comparison of the exact specific heat (continuous line) with the most probable levels approximation (dashed line) as a function of temperature for values of (a) the even number of particles $N = 2$ (red), 4 (orange), 10 (yellow) and 20 (green) and (b) the odd number of particles $N = 3$ (cyan), 5 (blue), 11 (purple), and 21 (black) for the antiferromagnetic case.

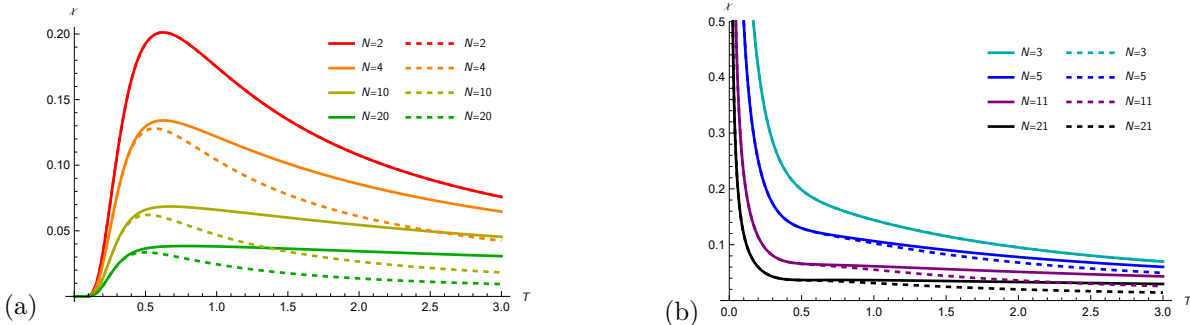


Figure 19: Comparison of the exact magnetic susceptibility (continuous line) with the most probable levels approximation (dashed line) as a function of temperature for values of (a) the even number of particle $N = 2$ (red), 4 (orange), 10 (yellow) and 20 (green) and (b) the odd number of particles $N = 3$ (cyan), 5 (blue), 11 (purple), and 21 (black) for the antiferromagnetic case.

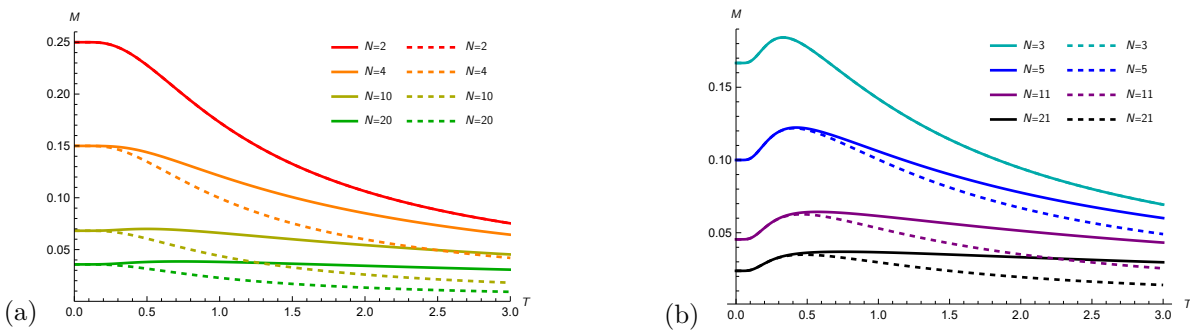


Figure 20: Comparison of the exact magnetisation (continuous line) with the most probable levels approximation (dashed line) as a function of temperature for values of (a) the even number of particles $N = 2$ (red), 4 (orange), 10 (yellow) and 20 (green) and (b) the odd number of particles $N = 3$ (cyan), 5 (blue), 11 (purple), and 21 (black) for the $h = \gamma = 1$ antiferromagnetic case.

We can see that the approximation is really good for small temperature values and that it worsens as this magnitude increases, as well as when the number of particles considered is larger. Therefore, as discussed in the following, this approximation allows us to describe the behaviour of thermodynamic quantities at low temperatures.

We return to the discussion of the thermodynamic quantities from the approximated analytical expressions. It is

clear from (25) that the magnetic susceptibility vanishes as T approaches zero for N even, since the dominant term is $1/(Te^{1/T})$, while for N odd it goes to infinity, going as $1/(4NT)$. Moreover, we can understand the magnetisation as a function of T , particularly for $T \rightarrow 0$. From (26), we find that in this limit, the magnetisation for N even is $3/(4(1+N))$, while for N odd is $1/(2N)$. Moreover, because the magnetic susceptibility diverges as T approaches zero, there are some “jumps” of the magnetisation at certain magnetic field values for zero temperature, as shown in Fig. 21. These can be obtained from the energy spectrum of Eq. (9).

We first consider the even case. From Eq. (9), it is easy to observe that the lowest energy state (and therefore the one relevant for zero temperature) in the absence of an external magnetic field will be $J = m = 0$. In this case, the magnetisation is zero because $m = 0$ is the only possible quantum number. When the external magnetic field increases, there is a value of $h = H_e^*(1)$ for which the lowest-energy state becomes that with $J = m = 1$. Therefore, a jump occurs for that value of the magnetic field. If the external magnetic field is increased again, up to $H_e^*(2)$, the lowest energy state will again be the one with one unit more of angular momentum, that is, $J = m = 2$. This process is repeated, and for a sufficiently high external magnetic field, the lowest energy state is the one with $J = m = N/2$.

For N odd, it is important to note that there is a jump at $h = h_o^*(1) = 0$. Without an external magnetic field, the lowest energy levels are those with the lowest angular momentum ($J = 1/2$); therefore, both states have the same energy. The total magnetisation of the system is zero because there is a cancellation between the two possible values of m . With a nonzero external magnetic field, the lowest-energy state is $J = m = 1/2$, and thus, a jump occurs. When the external field is increased, the same behaviour as that in the even case is observed.

The number of jumps in the magnetisation that occur depends on the number of particles for both N even and odd cases. In fact, there are $N/2$ or $(N+1)/2$ jumps, depending on whether N is even or odd, respectively. The spacing between transitions is one unit of the magnetic field (as can be seen from (9)), except for the spacing between the first and second jumps in the N odd case, which is $h_o^*(2) - h_o^*(1) = 3/2$ (remember that there is a phase transition in $h = h_o^*(1) = 0$). The values of the external magnetic field at which the jumps take place are given by the following equations

$$h_o^*(1) = 0, \quad h_o^*\left(\frac{n_o+1}{2}\right) = \frac{n_o}{2}, \quad \text{with} \quad n_o = 3, 5, \dots, N, \quad (27)$$

$$h_e^*\left(\frac{n_e}{2}\right) = \frac{n_e}{2}, \quad \text{with} \quad n_e = 2, 4, \dots, N. \quad (28)$$

Fig. 21 shows this magnetisation behaviour as a function of the external magnetic field for $N = 2, 3, 4, 5$.

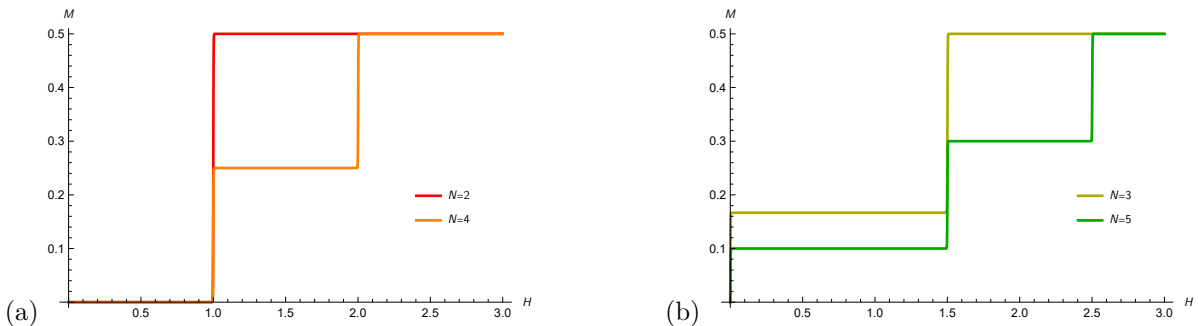


Figure 21: Magnetisation as a function of magnetic field for (a) even values of the number of particles $N = 2$ (red) and 4 (orange) and (b) odd values $N = 3$ (yellow), and 5 (green) for temperature $T = 0^+$, for the antiferromagnetic case.

4.2 Thermodynamic limit

Following this analysis, the behaviours of the properties described above were studied in the thermodynamic limit. In our case, the particle numbers $N = 100, 101, 500, 501, 1000$ and 1001 have been chosen, which are sufficiently large to study the thermodynamic limit.

In Fig. 22, we observe that, for a sufficiently high temperature, the behaviour of the specific heat for contiguous N tends to be the same, regardless of whether N is odd or even. We saw in Fig. 15 that saturation occurs after the maximum [11]. This effect is maintained and scaled for high N , so the thermodynamic limit curves are lowered for increasing N .

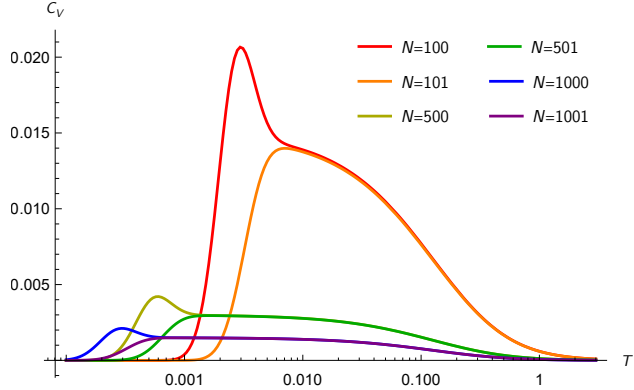


Figure 22: Specific heat as a function of temperature for values of the number of particles $N = 100$ (red), 101 (orange), 500 (yellow), 501 (green), 1000 (blue), and 1001 (purple), for the antiferromagnetic case.

As seen in [11], the specific heat tends to zero in the thermodynamic limit, and there is still a maximum, corresponding to the two lowest energy levels, even for N large. The behaviour decay $1/T^2$ is not observed, at least in the temperature range considered. For N high enough, the energy distribution of the energy levels is compressed and becomes proportional to N (as stated in [11]), so that the temperature range considered here ($T \in (0, 3)$) is sufficient to reach most of the highest energy levels. Thus, the system can hardly absorb more energy outside the considered temperature range.

It is important to note that the most probable levels for the specific heat in the thermodynamic limit are still those with $J = 0, 1$ for N even and $J = 1/2, 3/2$ for N odd. Taking the approach of just the two most probable levels, the analytic expressions of the specific heat in the thermodynamic limit are

$$C_V^{e,TL} = \frac{9e^{\frac{1}{NT}}}{N^3 T^2 \left(e^{\frac{1}{NT}} + 9 \right)^2}, \quad C_V^{o,TL} = \frac{9e^{\frac{3}{2NT}}}{N^3 T^2 \left(e^{\frac{3}{2NT}} + 4 \right)^2}. \quad (29)$$

In Fig. 23, it can be seen how the magnetic susceptibility converges to the thermodynamic limit (discussed in [11]), defined by the line at which every considered case tends. We can distinguish notably the N odd behaviour, which comes from above, from the N even behaviour, which comes from below. In [11], the nonzero thermodynamic limit of the magnetic susceptibility is analytically obtained. It is shown that the magnetic susceptibility behaviour of $N \rightarrow \infty$ can be expressed as $\chi = 1/(4T + 1)$.

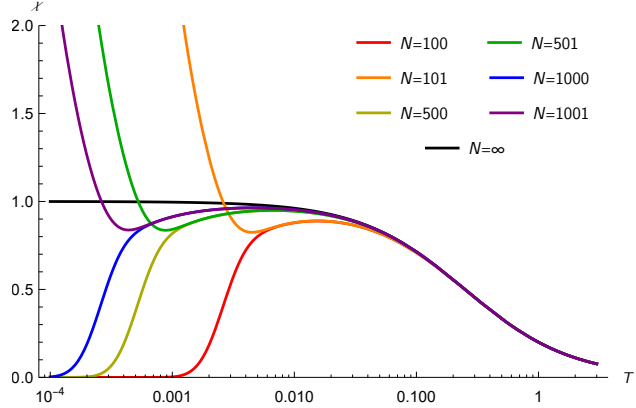


Figure 23: Magnetic susceptibility as a function of temperature for values of the number of particles $N = 100$ (red), 101 (orange), 500 (yellow), 501 (green), 1000 (blue), and 1001 (purple), for the antiferromagnetic case.

The change in coupling $I \rightarrow I/N$ does not imply changes in the most probable levels of the magnetic susceptibility once a magnetic field is applied, as this thermodynamic property is evaluated for a null field. Consequently, the most probable levels are still $J = 0, 1$ for even parity of N , and $J = 1/2, 3/2$ for odd parity of N . Then, the analytic expressions of magnetic susceptibility in the thermodynamic limit, taking the two most probable levels approximation, is as follows:

$$\chi^{e,TL} = \frac{6}{NT(9 + e^{\frac{1}{NT}})}, \quad \chi^{o,TL} = \frac{e^{\frac{3}{2NT}} + 20}{4NT(e^{\frac{3}{2NT}} + 4)}. \quad (30)$$

In Fig. 24, we present the magnetisation. We can see that all the N curves coincide in the thermodynamic limit.

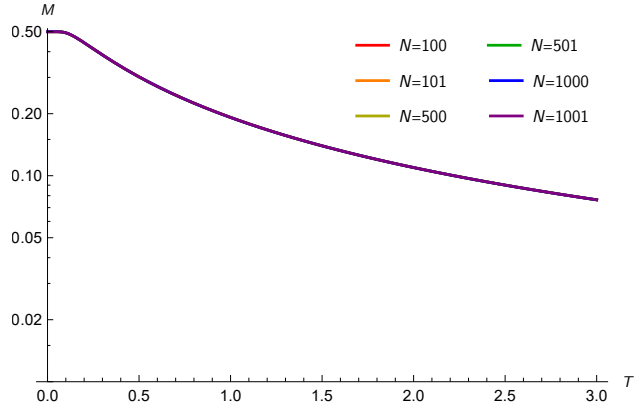


Figure 24: Magnetisation as a function of temperature for values of the number of particles $N = 100$ (red), 101 (orange), 500 (yellow), 501 (green), 1000 (blue), and 1001 (purple), for $h = \gamma = 1$ the antiferromagnetic case. They all are coincident.

In the presence of an external magnetic field, the fundamental states are $J = m = N/2$ and $J = m = N/2 - 1$, which are different from those in the ferromagnetic case. Every curve coincides in the thermodynamic limit owing to the change in the coupling constant $I \rightarrow I/N$. Contrary to the previous quantities, the most probable states change in the magnetisation for the thermodynamic limit because an external magnetic field is applied. Then, the magnetic part of expression (9) becomes the dominant term. For a small number of spins, we know that the minimum energy configuration is given by $J = m = 1/2$ in the odd N case and is shared between the $J = m = 0$ and $J = m = 1$ states in the even N case. Introducing the coupling change $I \rightarrow I/N$, the most probable state

becomes $J = m = N/2$ for any parity of N . This state is formed by N spins up and it dominates in the small temperature range. Thus, the magnetisation takes the value $M = 0.5$ at $T = 0$ and decreases once the next energy level is reached, because the maximum value of m decreases as J does. This uniform decrease persists for the same reasons as in the ferromagnetic case because the energy differences between states remain the same for different values of N . Using the approximation of the most probable levels ($J = N/2, N/2 - 1$), the following analytical expression is obtained:

$$M^{TL} = \frac{A - B - C + D + N}{E}, \quad (31)$$

where

$$\begin{aligned} A &= (N - 2)(N - 1)e^{\frac{3}{2T}}, \\ B &= N(N - 1)e^{\frac{5}{2T}}, \\ C &= (N + 2)e^{1/T}, \\ D &= e^{\frac{2N+1}{2T}} \left((N - 2)(N - 1) \left(-e^{1/T} \right) - Ne^{\frac{3}{2T}} + (N + 2)e^{\frac{1}{2T}} + N(N - 1) \right), \\ E &= 2N \left(e^{1/T} - 1 \right) \left(e^{\frac{1}{2T}} \left((N - 1)e^{1/T} - e^{N/T} \left(N + e^{\frac{1}{2T}} - 1 \right) \right) + 1 \right). \end{aligned}$$

As the antiferromagnetic expression, this is not very accurate at high temperatures, but it reasonably reproduces the magnetisation at low temperatures and during the transition.

In the previous graphs of the specific heat and magnetic susceptibility in the thermodynamic limit, it is important to note that the maxima are shifted to the left for increasing values of N . For large N , all the thermodynamic properties (24)–(26) converge to the same value, independent of the value of N , up to a $1/N$ factor. However, the interaction coupling I is replaced by I/N in the thermodynamic limit, which allows the displacement of the maxima. The magnetisation alone has coincident behaviour because the magnetic part becomes extremely dominant. Therefore, the behaviour of these quantities for larger N can be easily inferred from the presented plots.

The Curie temperature can now be obtained. Representing the inverse of the magnetic susceptibility, we find Fig. 25.

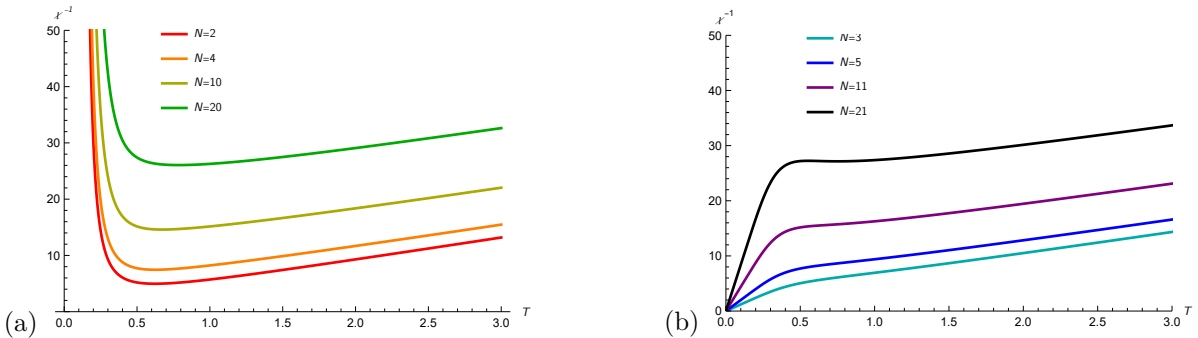


Figure 25: Inverse of magnetic susceptibility as a function of temperature for values of (a) the even number of particles $N = 2$ (red), 4 (orange), 10 (yellow) and 20 (green) and (b) the odd number of particles $N = 3$ (cyan), 5 (blue), 11 (purple), and 21 (black), for the antiferromagnetic case.

From the the analytic expression obtained previously, these are given by

$$\frac{1}{\chi^e} = \frac{9NT + (N + 4)e^{1/T}T}{6}, \quad \frac{1}{\chi^o} = \frac{4NT \left((N + 5)e^{\frac{3}{2T}} + 4(N - 1) \right)}{(N + 5)e^{\frac{3}{2T}} + 20(N - 1)}, \quad (32)$$

The even susceptibility does not diverge; therefore, it is not reasonable to calculate the Curie temperature in this case. In the odd case, the Curie temperature is $T_C = 0$ and the Curie constant is $C = \frac{1}{4N}$. It is important to note that in the thermodynamic limit, this would simply be an extension of what has been observed here and does not involve any particularly interesting discussion.

4.3 q -deformation for small number of spins

As discussed in the previous section, the main contribution to the thermodynamic quantities in the antiferromagnetic case is given by the two lowest-energy bands. In the q -deformed scenario, it is important to notice that $[1/2]_q[3/2]_q \rightarrow 1$ when $\eta(q) \rightarrow \infty$. Therefore, the term proportional to N in Eq. (13) is negligible for large values of η . As in the undeformed case, the main contributions are given by $J = 1/2, 3/2$ or $J = 0, 1$ for N odd or even, respectively. Then, we find the following approximated partition functions:

$$\begin{aligned}
Z_q^e &= e^{-\frac{2h-N\left[\frac{1}{2}\right]_q\left[\frac{3}{2}\right]_q+[2]_q+1}{2T}} \left(\left(\frac{N}{\frac{N}{2}}\right) e^{\frac{2h+[2]_q}{2T}} + \left(\frac{N}{\frac{N}{2}-1}\right) \left(-e^{\frac{2h+[2]_q}{2T}} + e^{\frac{2h+1}{2T}} + e^{\frac{4h+1}{2T}} + e^{\frac{1}{2T}}\right) - \right. \\
&\quad \left. - e^{\frac{1}{2T}} \left(\frac{N}{\frac{N}{2}-2}\right) \left(e^{h/T} + e^{\frac{2h}{T}} + 1\right)\right), \\
Z_q^o &= \left(e^{h/T} + 1\right) \left(\left(\frac{N}{\frac{N-5}{2}}\right) \left(e^{\frac{2h}{T}} + 1\right) e^{\frac{\left[\frac{1}{2}\right]_q\left[\frac{3}{2}\right]_q}{2T}} - \left(\frac{N}{\frac{N-3}{2}}\right) \left(e^{\frac{4h+\left[\frac{1}{2}\right]_q\left[\frac{3}{2}\right]_q}{2T}} - e^{\frac{2h+\left[\frac{3}{2}\right]_q\left[\frac{5}{2}\right]_q}{2T}} + e^{\frac{\left[\frac{1}{2}\right]_q\left[\frac{3}{2}\right]_q}{2T}}\right) - \right. \\
&\quad \left. - \left(\frac{N}{\frac{N-1}{2}}\right) e^{\frac{2h+\left[\frac{3}{2}\right]_q\left[\frac{5}{2}\right]_q}{2T}} \right) \left(-e^{\left(-\frac{3h-(N-1)\left[\frac{1}{2}\right]_q\left[\frac{3}{2}\right]_q+\left[\frac{3}{2}\right]_q\left[\frac{5}{2}\right]_q}{2T}\right)}\right). \tag{33}
\end{aligned}$$

Considering this argument, and as in the undeformed case, it was verified that the representations of the numerical results are faithfully reproduced with only the most probable levels in the antiferromagnetic case. Thus, we can obtain approximate analytic expressions for the specific heat as follows:

$$\begin{aligned}
C_{V,q}^e &= \frac{9(N+4)(q+1)^2 e^{\frac{q^2+1}{2T\sqrt{q}(1-q)}}}{4q \left(9NT e^{\frac{q^{3/2}}{2T(1-q)}} + (N+4)T e^{\frac{1}{2T\sqrt{q}(1-q)}}\right)^2} = \\
&= C_V^e + \frac{9(N+4)e^{1/T} \left((N+4)e^{1/T}(2T-1) + 9(2NT+N)\right)}{8T^3 \left((N+4)e^{1/T} + 9N\right)^3} (q-1)^2 + O((q-1)^3), \tag{34}
\end{aligned}$$

$$\begin{aligned}
C_{V,q}^o &= \frac{(N-1)(N+5) \left(q^2+q+1\right)^2 e^{\frac{(q+1)(q+\sqrt{q}+1)^2}{2(\sqrt{q}+1)^2 q T}}}{Nq^2T^2 \left((N+5)e^{\left(\frac{(1-q^{3/2})(1-q^{5/2})}{2(q-1)^2 q T}\right)} + 4(N-1)e^{\frac{q+\sqrt{q}+1}{2(\sqrt{q}+1)^2 T}}\right)^2} = \\
&= C_V^o + \frac{3(N-1)(N+5)e^{\frac{3}{2T}} \left((N+5)e^{\frac{3}{2T}}(4T-3) + 4(N-1)(4T+3)\right)}{2NT^3 \left((N+5)e^{\frac{3}{2T}} + 4(N-1)\right)^3} (q-1)^2 + O((q-1)^3). \tag{35}
\end{aligned}$$

The magnetic susceptibility is represented by

$$\begin{aligned}\chi_q^e &= \frac{6}{T \left((N+4)e^{\frac{q+1}{2\sqrt{q}T}} + 9N \right)} = \\ &= \chi^e - \frac{3(N+4)e^{\frac{1}{T}}}{4T^2 \left(Ne^{\frac{1}{T}} + 9N + 4e^{\frac{1}{T}} \right)^2} (q-1)^2 + O((q-1)^3),\end{aligned}\quad (36)$$

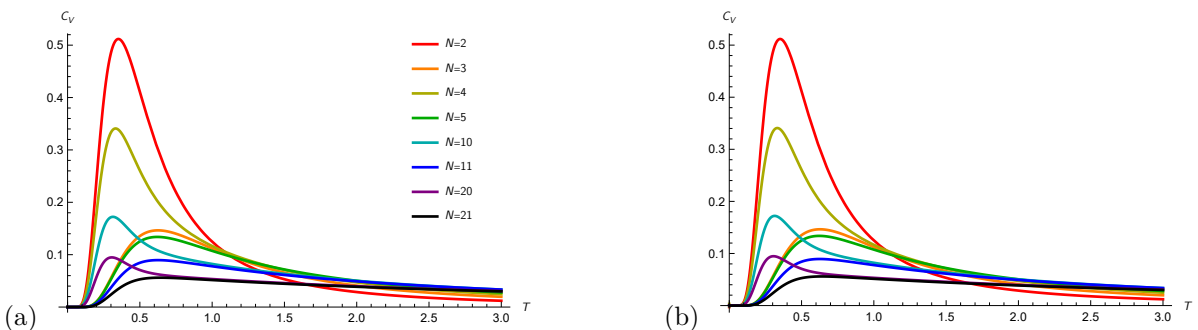
$$\begin{aligned}\chi_q^o &= \frac{(N+5)e^{\left(\frac{(1-q^{3/2})(1-q^{5/2})}{2(q-1)^2 q T} \right)}}{4NT \left((N+5)e^{\left(\frac{(1-q^{3/2})(1-q^{5/2})}{2(q-1)^2 q T} \right)} + 4(N-1)e^{\frac{q+\sqrt{q}+1}{2(\sqrt{q}+1)^2 T}} \right)} = \\ &= \chi^o - \frac{2(N^2 + 4N - 5)e^{\frac{3}{2}/T}}{NT^2 \left(Ne^{\frac{3}{2}/T} + 4N + 5e^{\frac{3}{2}/T} - 4 \right)^2} (q-1)^2 + O((q-1)^3).\end{aligned}\quad (37)$$

and the magnetisation is given by

$$\begin{aligned}M_q^e &= \frac{3e^{\frac{q^{3/2}}{2T(1-q)}} \left(e^{\frac{2}{T(1-q)}} - e^{\frac{2q}{T(1-q)}} \right)}{3Ne^{\frac{4+q^{3/2}}{2T(1-q)}} + 3Ne^{\frac{2(1+q)+q^{3/2}}{2T(1-q)}} + 3Ne^{\frac{q^{3/2}+4q}{2T(1-q)}} + (N+4)e^{\frac{2(1+q)+\frac{1}{\sqrt{q}}}{2T(1-q)}}} = \\ &= M^e - \frac{3(N+4)e^{2/T} (e^{2/T} - 1)}{8T \left(3Ne^{1/T} + 4(N+1)e^{2/T} + 3N \right)^2} (q-1)^2 + O((q-1)^3),\end{aligned}\quad (38)$$

$$\begin{aligned}M_q^o &= \frac{(N+5) \left(e^{\frac{1}{T}} - 1 \right) e^{\left(\frac{1}{T} + \frac{(1-q^{3/2})(1-q^{5/2})}{2q(q-1)^2 T} \right)}}{2N \left(e^{\frac{1}{T}} + 1 \right) \left((N+5)e^{\left(\frac{1}{T} + \frac{(1-q^{3/2})(1-q^{5/2})}{2q(q-1)^2 T} \right)} + 2(N-1)e^{\frac{q+\sqrt{q}+1}{2(\sqrt{q}+1)^2 T}} \left(-e^{\frac{1}{T}} + e^{\frac{2}{T}} + 3e^{\frac{3}{T}} - 3 \right) \right)} = \\ &= M^o - \frac{(N^2 + 4N - 5)e^{\frac{5}{2}/T} (e^{\frac{1}{T}} - 1) (e^{\frac{1}{T}} + 1)}{NT \left(2Ne^{2/T} + Ne^{\frac{5}{2}/T} + 2N - 2e^{2/T} + 5e^{\frac{5}{2}/T} - 2 \right)^2} (q-1)^2 + O((q-1)^3).\end{aligned}\quad (39)$$

We now represent the exact thermodynamic quantities using numerical methods. We start by considering the specific heat, as shown in Fig. 26 as a function of η .



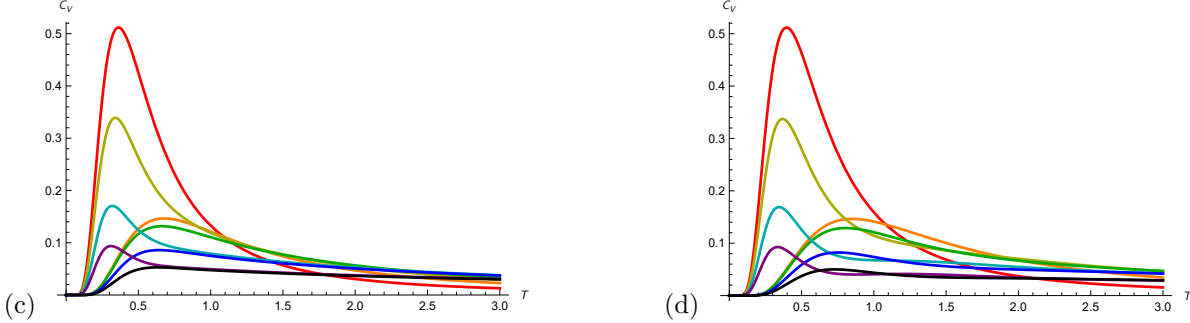


Figure 26: Specific heat as a function of temperature for values of the number of particles $N = 2$ (red), 3 (orange), 4 (yellow), 5 (green), 10 (cyan), 11 (blue), 20 (purple), and 21 (black) and of the parameter (a) $\eta = 0$, (b) $\eta = 0.1$, (c) $\eta = 0.5$, and (d) $\eta = 1$, for the antiferromagnetic case.

It can be observed that the representation for $\eta = 0$ is exactly the same as that for the undeformed case previously presented. The values of the maxima for different N are the same as in the undeformed case, and the different behaviours when N is even or odd are preserved. Moreover, one can observe that the peak moves to the right as the parameter η increases because the energy corresponding to the second lowest angular momentum becomes larger. This implies that the peaks for $\eta = 0$ are placed farthest to the left.

Regarding the magnetic susceptibility, Fig. 27 was obtained for different values of η . We observe that the maxima for N even become smaller as η increases, and for N odd, the behaviour of $1/(NT)$ does not change as a function of η for high values of T .

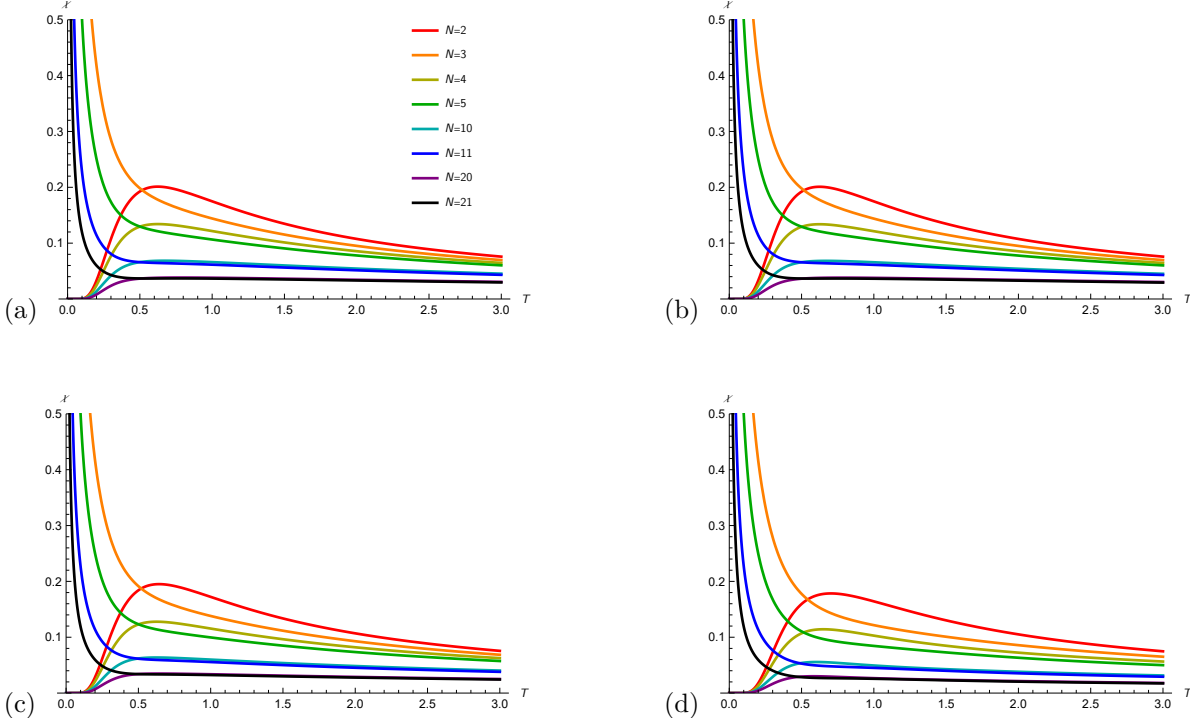


Figure 27: Magnetic susceptibility as a function of temperature for values of the number of particles $N = 2$ (red), 3 (orange), 4 (yellow), 5 (green), 10 (cyan), 11 (blue), 20 (purple), and 21 (black) and of the parameter (a) $\eta = 0$, (b) $\eta = 0.1$, (c) $\eta = 0.5$, and (d) $\eta = 1$, for the antiferromagnetic case.

The maxima of N even, which become smaller with increasing η , can be easily understood as follows. The energy of different states, except for the fundamental state, exponentially increases as the deformation parameter

increases; therefore, they become less probable. Consequently, in the observed peaks corresponding to the transition from the ground state to the first excited state, the probability weight of the ground state is larger.

Finally, we compute the magnetisation in the presence of an external magnetic field in Fig. 28. Here, we can observe an interesting feature: there is a completely different behaviour for N odd or even when increasing η . For N odd, the bump near zero temperature (commented in the previous section) disappears with the η parameter large enough, the value at zero temperature being the same as in the undeformed case. For N even, the maxima are shifted to the right and become smaller, and the magnetisation vanishes at zero temperature for $\eta \neq 0$.

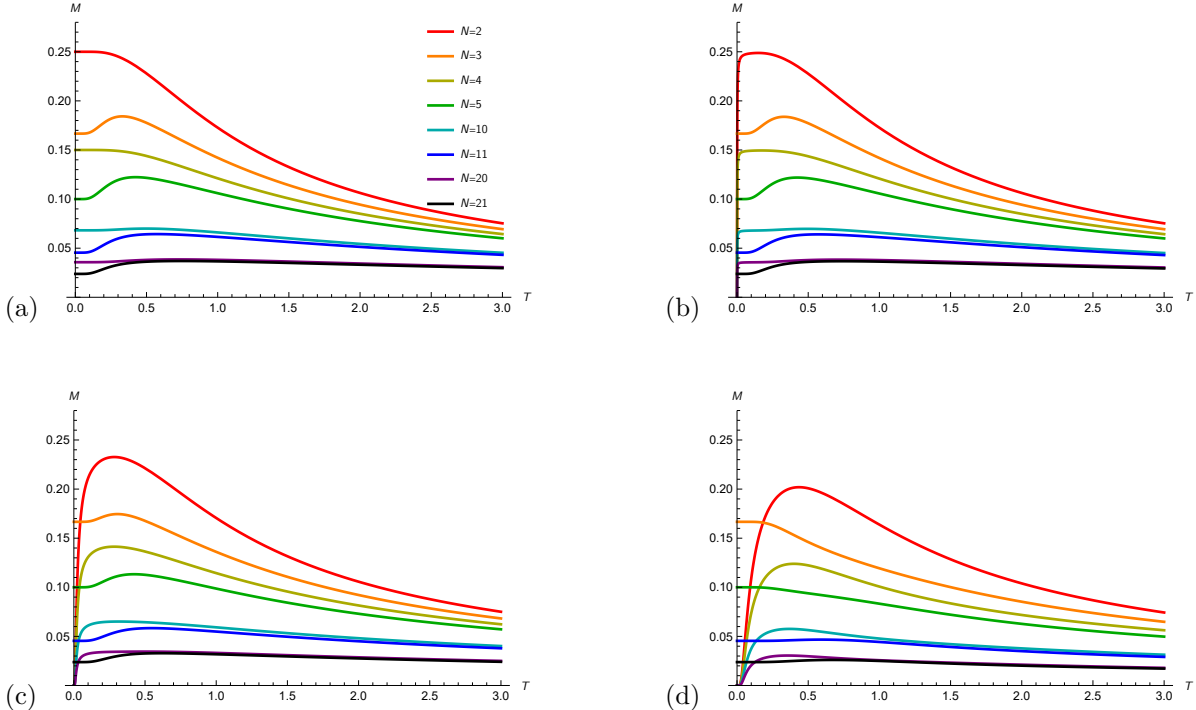


Figure 28: Magnetisation as a function of temperature for values of the number of particles $N = 2$ (red), 3 (orange), 4 (yellow), 5 (green), 10 (cyan), 11 (blue), 20 (purple), and 21 (black) and of the parameter (a) $\eta = 0$, (b) $\eta = 0.1$, (c) $\eta = 0.5$, and (d) $\eta = 1$ for the $h = \gamma = 1$ antiferromagnetic case.

We can now try to understand the behaviour of the magnetisation observed above for $h = 1$ as a function of the deformation parameter q . As before, to understand this, we consider the $N = 2$ and $N = 3$ cases for a generic deformation parameter q . For the first case, one finds that the minimum energy state is not shared by the two configurations as in the undeformed scenario, but it is given by one spin up and one spin down with $J = m = 0$ (and energy $-[1/2]_q [3/2]_q$). The next energy level is given by two spins up with $J = m = 1$ (and energy $1/2([2]_q - [1/2]_q [3/2]_q - 2)$). This last configuration comes into play when the temperature is sufficiently increased and, consequently, the magnetisation increases to the observed peak in every N even case. When the temperature continues to increase, all possible configurations are averaged, and the magnetisation goes to zero.

As discussed above, for N even, the magnetisation vanishes at zero temperature when a deformation is applied. In the undeformed model, a jump occurs at zero temperature and magnetic field $h = 1$. However, in the deformed case, with $q \neq 1$, the same jump occurs for a magnetic field value larger than $h = 1$ (see discussion below for the exact values of the magnetic field at which the jumps occur as a function of the deformation parameter). Therefore, the magnetisation for N even is null because the first jump does not take place at $h = 1$.

In the $N = 3$ case, the minimum energy configuration is the same as in the undeformed case: two spins up and one spin down with $J = m = 1/2$ (and energy $-[1/2]_q [3/2]_q - 1/2$). This explains why the magnetisation in odd N cases starts from the same value for both deformed and undeformed scenarios, independently of the value of q . However, the first excited state varies as a function of the deformation parameter η . When it belongs to the interval $\eta \in [0, 0.9625]$, this state is the same as in the undeformed case: the three spins up with $J = m = 3/2$ (and

energy $1/2([3/2]_q [5/2]_q - 3 [1/2]_q [3/2]_q) - 3/2$). Thus, it can be observed that for the representations of $\eta = 0.1$ and $\eta = 0.5$, there is a small peak when the temperature is slightly increased, as this state has greater magnetisation. However, when the deformation parameter is greater than the critical value, that is, for $\eta > 0.9625$, the second lowest energy state is given by two spins down and one spin up with $J = m = 1/2$ (with energy $-[1/2]_q [3/2]_q + 1/2$). This configuration does not increase the magnetisation; therefore, for $\eta = 1$ this quantity decreases smoothly from its initial value at a small temperature and then goes to zero as the temperature increases. The same explanation can be applied for all N odd cases.

The value of the magnetisation at zero temperature for N odd can also be understood by examining the magnetisation values at which the jumps occur. Since the first jump of the magnetisation for both deformed and undeformed cases takes place first at $h = 0$, the magnetisation at zero temperature for N odd has the same value as the undeformed case.

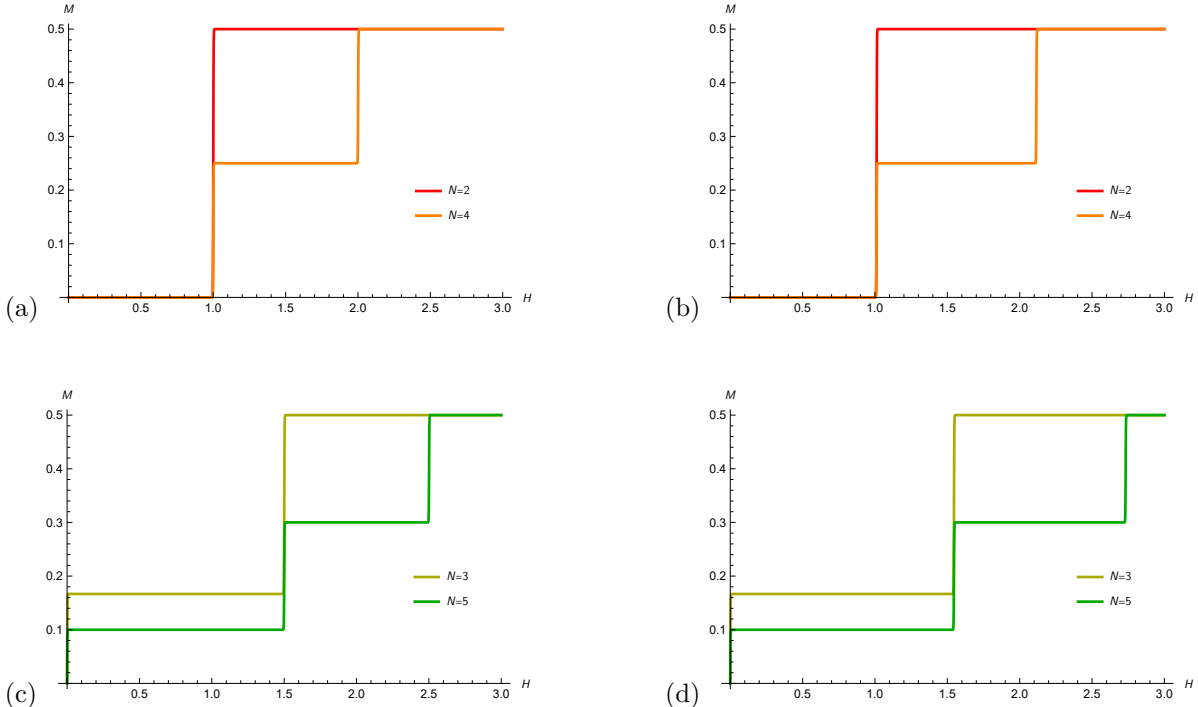


Figure 29: Magnetisation as a function of magnetic field for values of the number of particles and of the parameter η for temperature $T = 0^+$, for the antiferromagnetic case. The representations (a) and (b) represent the even number of particles $N = 2$ (red) and 4 (orange) for $\eta = 0$, $\eta = 0.3$ respectively, while (c) and (d) represent the odd number of particles $N = 3$ (yellow) and 5 (green) for $\eta = 0$, $\eta = 0.3$ respectively.

The number of jumps in the magnetisation that occur depends exactly as in the undeformed case on the number of particles: there are $N/2$ or $(N+1)/2$ phase transitions depending on whether N is even or odd, respectively. The difference with respect to the undeformed case is due to the spacing between transitions, because the energies for different angular momenta are not given by (9) but (13). As before, by computing the difference between contiguous energy levels from (13) it is easy to obtain the values of the external magnetic field at which the jumps take place

$$h_o^*(1) = 0, \quad h_o^*\left(\frac{n_o+1}{2}\right) = \frac{[n_o]_q}{2}, \quad \text{with} \quad n_o = 3, 5, \dots, N, \quad (40)$$

$$h_e^*\left(\frac{n_e}{2}\right) = \frac{[n_e]_q}{2}, \quad \text{with} \quad n_e = 2, 4, \dots, N. \quad (41)$$

Of course, when taking the limit $q \rightarrow 1$ one finds the same expressions (27)–(28) obtained in the previous section.

As can be seen in Fig. 29, all jumps tend to move to the right, except for the first one (for zero magnetic field) in the N odd case because, as commented above, the minimum energy configuration is shared by two states whose

average magnetisation is zero. When a magnetic field is applied, the state with the highest m becomes the one with the minimum energy; thus, a jump occurs at $H_o^*(1) = 0$.

4.4 q -deformation of the thermodynamic limit

As in the undeformed scenario, we can study the thermodynamic limit in the deformed case. In addition to the modifications observed for small N , when the value of the deformation parameter increases, the convergence between contiguous N (with different parity) requires a higher temperature.

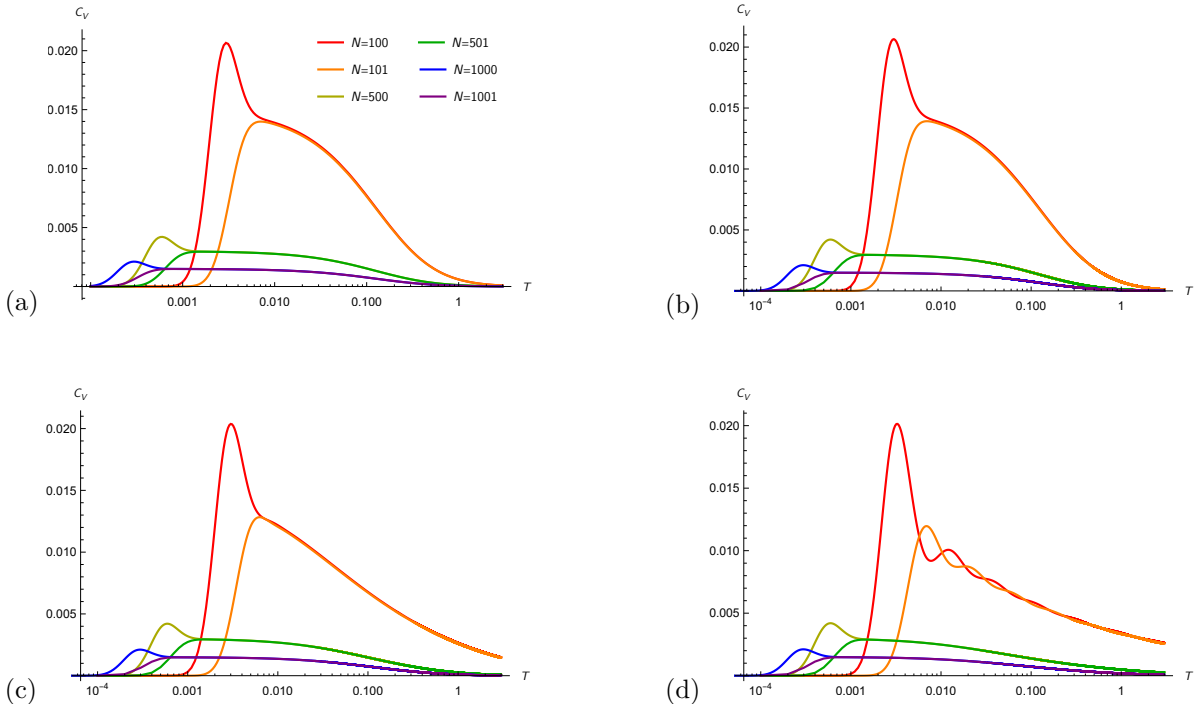


Figure 30: Specific heat as a function of temperature for values of the number of particles $N = 100$ (red), 101 (orange), $N = 500$ (yellow), 501 (green), $N = 1000$ (blue), 1001 (purple) for the antiferromagnetic case. The values of the parameter $q = e^{\eta/N}$ are: (a) $\eta = 0$, (b) $\eta = 10$, (c) $\eta = 50$, and (d) $\eta = 100$.

First, as in the undeformed case, the maxima are shifted to the left for increasing values of N (for the same q). In particular, in Fig. 30 (d), several bumps can be observed for both the even and odd N cases, which become less sharp as the temperature increases. These are due to transitions between consecutive J energy levels. These transitions overlap in the undeformed case; however, as explained previously, the energy required to reach the excited levels increases when deformation is introduced. By plotting the most probable levels, it can be seen that these bumps are due to the transitions between consecutive J -energetic levels. Every transition occurs at higher temperatures as η increases because the difference between each pair of energy levels is also greater. These bumps are more pronounced and smaller with increasing values of the deformation parameter because the deformation becomes more visible at high temperatures. This occurs because the deformation increases the energy differences between levels, as seen in [53], and thus the transitions are visible at higher temperatures. The decrease in the magnitude can be understood from the fact that although the first fundamental states have less energy when the deformation parameter is increased, the energy of the next excited levels becomes exponentially larger. Therefore, the lowest-energy states become more likely, and the total energy of the system is closer to the energy of the lowest level. This implies that the specific heat exhibits smaller bumps for larger values of η .

In the deformed case, the most probable levels for any number of particles are the same as in the undeformed scenario ($J = 0, 1$ for N even and $J = 1/2, 3/2$ for N odd). Consequently, we can also get the analytic expressions

of specific heat in the deformed case

$$\begin{aligned}
C_{V,q}^{e,TL} &= \frac{9(q+1)^2 e^{\frac{q^{3/2} + \frac{1}{\sqrt{q}}}{2NT(1-q)}}}{4N^3 q T^2 \left(9e^{\frac{q^{3/2}}{2NT(1-q)}} + e^{\frac{1}{2NT\sqrt{q}(1-q)}} \right)^2} = \\
&= C_V^{e,TL} + \frac{9e^{\frac{1}{NT}} \left(18NT + e^{\frac{1}{NT}} (2NT - 1) + 9 \right)}{8N^4 T^3 \left(e^{\frac{1}{NT}} + 9 \right)^3} (q-1)^2 + O((q-1)^3), \tag{42}
\end{aligned}$$

$$\begin{aligned}
C_{V,q}^{o,TL} &= \frac{(q^2 + q + 1)^2 e^{\frac{(q+1)(q+\sqrt{q}+1)^2}{2N(\sqrt{q}+1)^2 q T}}}{N^3 q^2 T^2 \left(e^{\frac{(1-q^{3/2})(1-q^{5/2})}{2N(q-1)^2 q T}} + 4e^{\frac{q+\sqrt{q}+1}{2N(\sqrt{q}+1)^2 T}} \right)^2} = \\
&= C_V^{o,TL} + \frac{3e^{\frac{3}{NT}} (4NT - 3) + 12e^{\frac{3}{2NT}} (4NT + 3)}{2N^4 T^3 \left(e^{\frac{3}{2NT}} + 4 \right)^3} (q-1)^2 + O((q-1)^3). \tag{43}
\end{aligned}$$

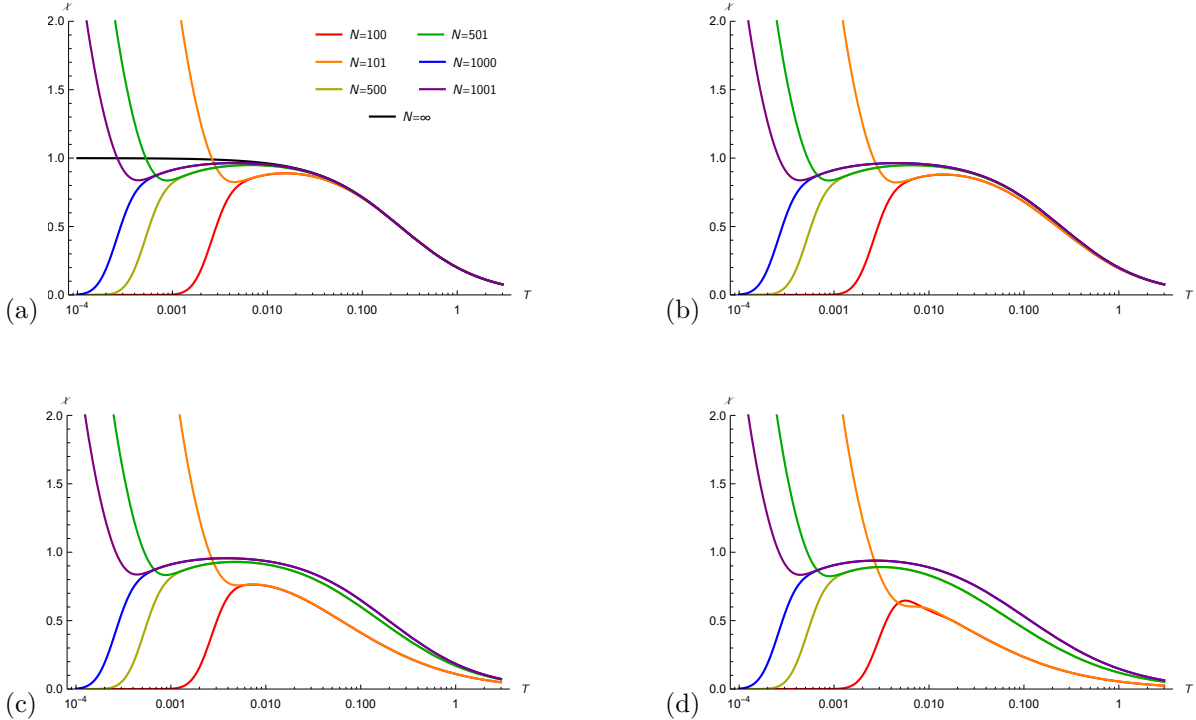


Figure 31: Magnetic susceptibility as a function of temperature for values of the number of particles $N = 100$ (red), 101 (orange), $N = 500$ (yellow), 501 (green), $N = 1000$ (blue), 1001 (purple) for the antiferromagnetic case. The values of the parameter $q = e^{\eta/N}$ are: (a) $\eta = 0$, (b) $\eta = 10$, (c) $\eta = 50$, and (d) $\eta = 100$.

For the magnetic susceptibility, the convergence observed in the undeformed case is attenuated, as shown in Fig. 31. As deformation is introduced, the curves require a higher temperature to converge and practically do so for a zero value of the susceptibility. Moreover, as in the undeformed case, the curves shift to the left for increasing values of N (for the same q).

As in the undeformed case, the most probable levels of magnetic susceptibility are the same as for the specific heat ($J = 0, 1$ for N even and $J = 1/2, 3/2$ for N odd). This fact allows us to obtain analytic expressions of the

magnetic susceptibility in the deformed case

$$\chi_q^{e,TL} = \frac{6}{NT(e^{\frac{q+1}{2N\sqrt{q}T}} + 9)} = \chi^{e,TL} - \frac{3e^{\frac{1}{NT}}}{4N^2T^2(e^{\frac{1}{NT}} + 9)^2}(q-1)^2 + O((q-1)^3), \quad (44)$$

$$\chi_q^{o,TL} = \frac{e^{\frac{q^4+1}{2N(q-1)^2qT}} + 20e^{\frac{q^2+1}{2N(q-1)^2T}}}{4NT(e^{\frac{q^4+1}{2N(q-1)^2qT}} + 4e^{\frac{q^2+1}{2N(q-1)^2T}})} = \chi^{o,TL} - \frac{2e^{\frac{3}{2NT}}}{N^2T^2(e^{\frac{3}{2NT}} + 4)^2}(q-1)^2 + O((q-1)^3). \quad (45)$$

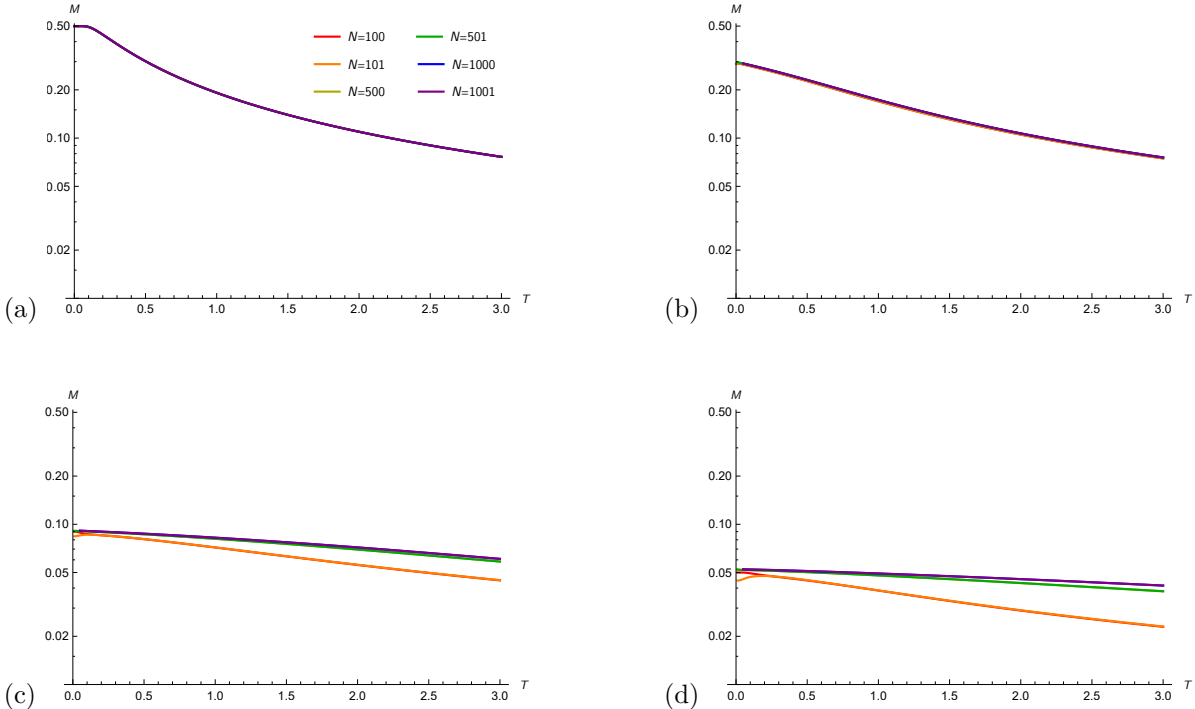


Figure 32: Magnetisation as a function of temperature for values of the number of particles $N = 100$ (red), 101 (orange), $N = 500$ (yellow), 501 (green), $N = 1000$ (blue), 1001 (purple), for the $h = \gamma = 1$ antiferromagnetic case. The values of the parameter $q = e^{\eta/N}$ are: (a) $\eta = 0$, (b) $\eta = 10$, (c) $\eta = 50$, and (d) $\eta = 100$.

For magnetisation, the most probable levels are not the same as those obtained for the specific heat and magnetic susceptibility because an external magnetic field is applied. In fact, they are not even the same levels for every value of the deformation parameter. To describe them, we obtained an equation that allows us to obtain the most probable levels from the deformation parameter and the number of particles. This is obtained by minimizing the energy expression with an external magnetic field (13) (for $h = \gamma = 1$ and $m = J$) as a function of J

$$J_{MP} = m_{MP} = \frac{N \cdot \operatorname{arcsinh} \left(\frac{2N^2(\cosh(\eta/N)-1)}{\eta} \right)}{\eta} - \frac{1}{2}. \quad (46)$$

The two most probable energy states are those with angular momentum being the closest integers for even N and the closest semi-integer for odd N . From them, we would also be able to write the analytical approximation carried out for the undeformed case. However, because the most probable states depend on N , we cannot write a generic expression as we did previously.

Owing to the dependence of the most probable levels on the number of particles and the value of the deformation parameter, the deformed magnetisation at $T = 0$ has different values for different q and N , as shown in Figs. 32 (b), (c), and (d). These magnetisation values at zero temperature can be calculated using (46): $M(T = 0) = m_{MP}/N$.

We show the computation of the most probable states (magnetisation at zero temperature) for three deformation values in Table 1.

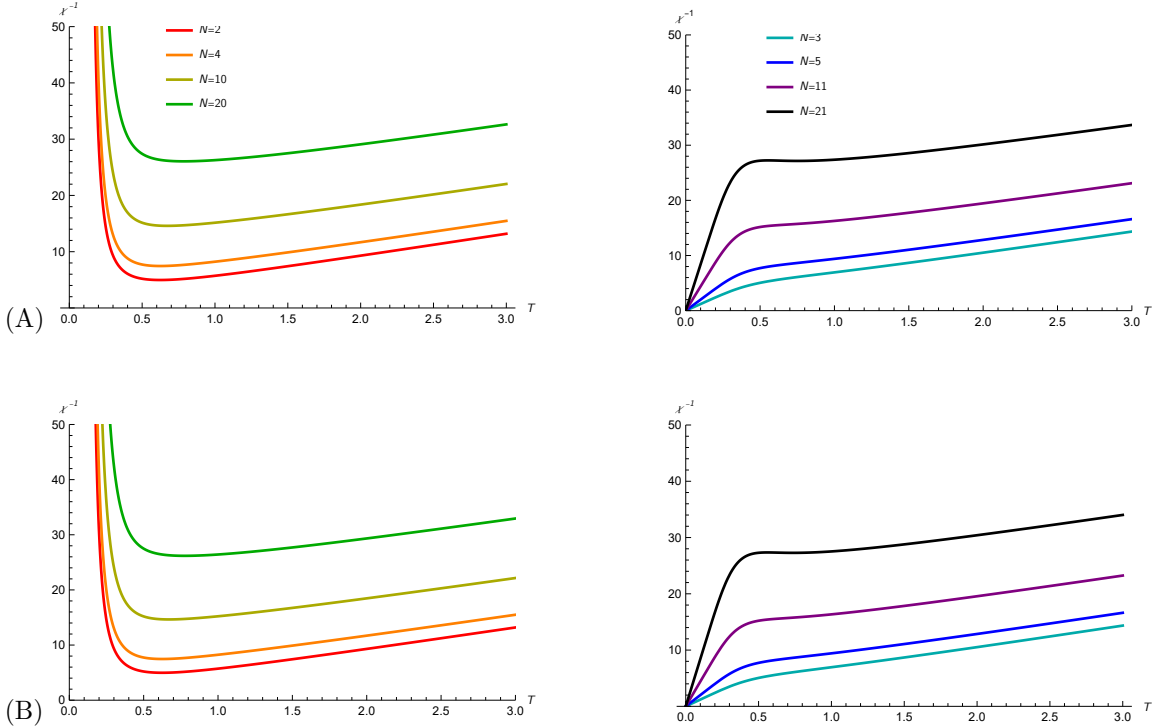
N	$ J_{MP}, m_{MP}\rangle_{q=e^{10/N}}$	$ J_{MP}, m_{MP}\rangle_{q=e^{50/N}}$	$ J_{MP}, m_{MP}\rangle_{q=e^{100/N}}$
100	$ 29, 29\rangle$	$ 9, 9\rangle$	$ 5, 5\rangle$
101	$ 29.5, 29.5\rangle$	$ 8.5, 8.5\rangle$	$ 4.5, 4.5\rangle$
500	$ 149, 149\rangle$	$ 46, 46\rangle$	$ 26, 26\rangle$
501	$ 149.5, 149.5\rangle$	$ 45.5, 45.5\rangle$	$ 26.5, 26.5\rangle$
1000	$ 299, 299\rangle$	$ 92, 92\rangle$	$ 52, 52\rangle$
1001	$ 299.5, 299.5\rangle$	$ 91.5, 91.5\rangle$	$ 52.5, 52.5\rangle$

Table 1: Data for different number of particles of the most probable states in presence of an external magnetic field $h = \gamma = 1$.

The curves associated with an odd number of particles demonstrate an initial increase at lower temperatures, followed by a subsequent decrease. This behavior can be explained by the energy distribution, where, for an odd number of particles, the first excited state corresponds to the next consecutive magnetic quantum number m . This leads to a slight increase in magnetisation. In contrast, for an even number of particles, the first excited state corresponds to the previous consecutive magnetic quantum number m , resulting in a decrease in the magnetisation.

In addition, the decrease in magnetisation becomes more gradual as the deformation parameter increases. This is again due to the fact that the deformed systems require more energy to reach the excited states. Consequently, the magnetisation behaviour is dominated by the most probable states.

We can now obtain the Curie temperature. We begin by representing the inverse of the magnetic susceptibility in Fig. 33 for different values of q .



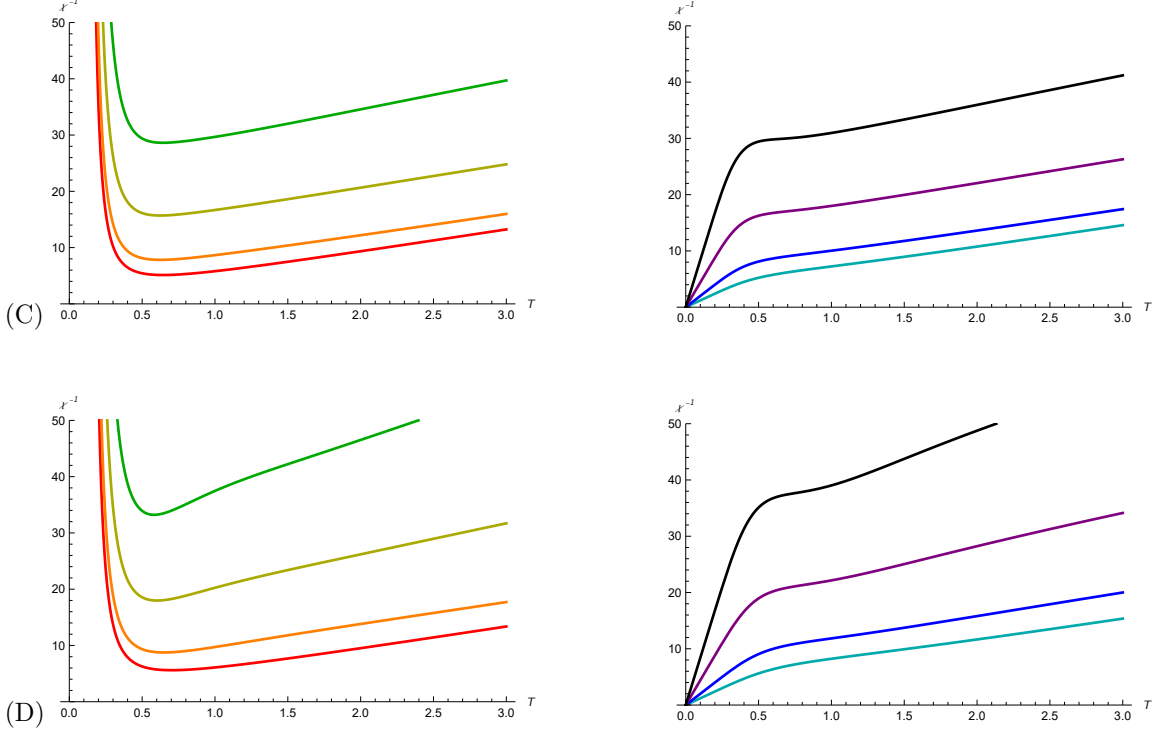


Figure 33: Inverse of magnetic susceptibility as a function of temperature for values of (A) the even number of particles $N = 2$ (red), 4 (orange), 10 (yellow) and 20 (green) and (B) the odd number of particles $N = 3$ (cyan), 5 (blue), 11 (purple), and 21 (black), and of the parameter (A) $\eta = 0$, (B) $\eta = 0.1$, (C) $\eta = 0.5$, and (D) $\eta = 1$, for the antiferromagnetic case.

Taking the analytic expressions of the most probable states we find

$$\frac{1}{\chi^e} = \frac{T \left((N+4)e^{\frac{q+1}{2\sqrt{q}T}} + 9N \right)}{6}, \quad (47)$$

$$\frac{1}{\chi^o} = \frac{4NT \left((N+5)e^{\left(\frac{(1-q^{3/2})(1-q^{5/2})}{2(q-1)^2 q T} \right)} + 4(N-1)e^{\frac{q+\sqrt{q}+1}{2(\sqrt{q}+1)^2 T}} \right)}{(N+5)e^{\left(\frac{(1-q^{3/2})(1-q^{5/2})}{2(q-1)^2 q T} \right)} + 20(N-1)e^{\frac{q+\sqrt{q}+1}{2(\sqrt{q}+1)^2 T}}}, \quad (48)$$

The even susceptibility does not diverge, so it does not make sense to calculate the Curie temperature in this case. In the odd case, the Curie temperature is $T_C = 0$ and the Curie constant is $C = \frac{1}{4N}$, exactly as in the undeformed case.

5 Conclusions

In this work, the main thermodynamical properties of the q -deformation of the KS model were investigated. Introducing the quantum algebra $\mathfrak{su}_q(2)$, the main properties analysed in [11] for the KS model are studied here for its q -deformed version. In particular, for the q -deformed KS Hamiltonian, we studied the specific heat, magnetic susceptibility, magnetisation, phase transitions, and Curie temperature.

In the ferromagnetic case, we cannot deduce approximate analytical expressions for the thermodynamic quantities. The difference with respect to the antiferromagnetic case, for which we were able to do it, is that the distance

between the smallest energy levels tends to zero in the antiferromagnetic case. However, this distance is not negligible in the ferromagnetic case. This implies that the specific heat shows its maximum at a significantly higher temperature for larger N , in contrast to the antiferromagnetic case. Therefore, while the approximation of considering the two lowest energy levels reproduces the behaviour of the specific heat at low temperatures, it cannot describe the maximum, since it is at a higher temperature at which the approximation is not valid.

When considering the thermodynamic limit, the change in the coupling $I \rightarrow I/N$ causes the energy distribution to compress. This modification, combined with a deformation inversely proportional to the number of particles, ensures the extensibility of the model. In the undeformed case, the behaviour has a slightly pronounced dependence on the number of particles: in the specific heat, the peaks are similar in magnitude and occur at the same temperature; in susceptibility, the Curie transition occurs at nearly the same temperature; and in magnetisation, the curves are practically identical. Conversely, in the deformed case, the behaviour changes drastically. Therefore, careful consideration is required when selecting the values of the deformation parameter. In this study, particularly small values of q were chosen, which were significantly smaller than those used in the antiferromagnetic case, to observe progressive changes. In all three thermodynamic functions, a shift in behaviour toward higher temperatures was observed when deformation was introduced.

In the antiferromagnetic case, by considering the most probable levels, we can find a reasonable and useful approximation to obtain analytical expressions for both undeformed and deformed scenarios, from which we can understand the behaviour of the thermodynamic quantities and phase transitions. Moreover, we can find (exact) analytical expressions of the magnetic field at which phase transitions occur for both deformed and undeformed cases, which is a study not explored in [11]. The most appreciable change between the deformed and undeformed cases is observed in the magnetisation, particularly in the jumps at zero temperature as a function of the external magnetic field.

We also discussed the thermodynamic limit of the antiferromagnetic case. We observe that the analytical expressions of the thermodynamic quantities considered converge to be the same, up to a factor $1/N$, for both undeformed and deformed cases. This remarkable tendency disappears when deformation is introduced. The distribution of the energy states changes in the deformed case. Specifically, the excitation energies increase under deformation, so accessing the excited states requires more energy than in the undeformed case, which enhances the relative stability of the ground states. Consequently, the convergence may not disappear, but it would occur at temperatures higher than those considered, for which the susceptibility becomes very small (compared to its value at low temperatures).

Finally, we discuss the possible applications of this deformation. When introducing the q deformation, the spins are not coupled identically, and this is why the thermodynamic quantities vary with respect to the undeformed case (this is indeed the reason why the phase transitions are shifted to a higher value of the magnetic field). Therefore, while the Kittel-Shore model provides a robust framework for describing equidistant spin systems characterised by isotropic exchange, its deformation could take care of modifications in distance or anisotropic exchange, which is particularly relevant for ultrasmall clusters such as ammonia in quantum computation [58]. Our deformed model builds upon established literature concerning organic molecules with embedded paramagnetic ions, where weak intermolecular interactions allow for individual magnetic descriptions. As demonstrated in previous research, this approach facilitates the derivation of analytical expressions for total magnetic moments and spin-correlation functions in specific geometries, including dimers, equilateral triangles, squares, and regular or irregular tetrahedrons [23, 59, 60], while also accounting for melting anomalies in systems such as H_2O in porous Al_2O_3 [61]. The model further integrates effectively with thermodynamic frameworks to estimate the efficiency of nickel-based multiferroic thermomagnetic generators (MTMG) and Curie point suppression in ferromagnetic nanosolids [62–64]. By utilizing the “equal access” random-phase approximation (EA-RPA) scheme, the KS model remains consistent with magnetization studies in copper oxide antiferromagnets like La_2CuO_4 and $\text{YBa}_2\text{Cu}_3\text{O}_6$ [65–67], as well as in determining scattering cross-sections for isotropic disordered magnets [68]. Consequently, our findings underscore the versatility of the KS model in bridging theoretical spin dynamics with practical applications in nanomaterials and quantum thermodynamics. This opens a new branch of study that we hope to explore in our future work.

Acknowledgments

The authors appreciate the useful discussions with Ángel Ballesteros, Nicolás Cordero, and Ivan Gutierrez-Sagredo. This work has been partially supported by Agencia Estatal de Investigación (Spain) under grant PID2019-106802GB-I00/AEI/10.13039/501100011033, by the Regional Government of Castilla y León (Junta de Castilla y León, Spain), and by the Spanish Ministry of Science and Innovation MICIN and the European Union NextGenerationEU (PRTR C17.I1). The authors would like to acknowledge the contribution of the COST Action CA23130. The authors have benefited from the activities of COST Action CA23115: Relativistic Quantum Information, funded by COST (European Cooperation in Science and Technology).

References

- [1] C. Kittel and H. Shore. Development of a Phase Transition for a Rigorously Solvable Many-Body System. *Physical Review*, 138:A1165–A1169, 5 1965. [doi:10.1103/PhysRev.138.A1165](https://doi.org/10.1103/PhysRev.138.A1165).
- [2] H. Capel. On the possibility of first-order transitions in Ising systems of triplet ions with zero-field splitting III. *Physica*, 37:423–441, 1 1967. [doi:10.1016/0031-8914\(67\)90198-X](https://doi.org/10.1016/0031-8914(67)90198-X).
- [3] J. F. Nagle and J. C. Bonner. Numerical studies of the Ising chain with long-range ferromagnetic interactions. *Journal of Physics C: Solid State Physics*, 3:352–366, 2 1970. [doi:10.1088/0022-3719/3/2/017](https://doi.org/10.1088/0022-3719/3/2/017).
- [4] M. Suzuki. Relationship between d -Dimensional Quantal Spin Systems and $(d + 1)$ -Dimensional Ising Systems: Equivalence, Critical Exponents and Systematic Approximants of the Partition Function and Spin Correlations. *Progress of Theoretical Physics*, 56:1454–1469, 11 1976. [doi:10.1143/PTP.56.1454](https://doi.org/10.1143/PTP.56.1454).
- [5] H. F. Trotter. On the product of semi-groups of operators. *American Mathematical Society*, 545:10, 1959.
- [6] A. J. van der Sijs. Heisenberg models and a particular isotropic model. *Physical Review B*, 48:7125–7133, 9 1993. [doi:10.1103/PhysRevB.48.7125](https://doi.org/10.1103/PhysRevB.48.7125).
- [7] A. Czachor. A verification of the random-phase-approximation using exact thermodynamic functions for the Kittel–Shore–Kac model magnet. *Physica B: Condensed Matter*, 311:56–60, 1 2002. [doi:10.1016/S0921-4526\(01\)01056-0](https://doi.org/10.1016/S0921-4526(01)01056-0).
- [8] R. Botet, R. Jullien, and P. Pfeuty. Size Scaling for Infinitely Coordinated Systems. *Physical Review Letters*, 49:478–481, 8 1982. [doi:10.1103/PhysRevLett.49.478](https://doi.org/10.1103/PhysRevLett.49.478).
- [9] R. Botet and R. Jullien. Large-size critical behavior of infinitely coordinated systems. *Physical Review B*, 28:3955–3967, 10 1983. [doi:10.1103/PhysRevB.28.3955](https://doi.org/10.1103/PhysRevB.28.3955).
- [10] J. L. Cardy. *Introduction to Theory of Finite-Size Scaling*, volume 2, pages 1–7. 1988. [doi:10.1016/B978-0-444-87109-1.50006-6](https://doi.org/10.1016/B978-0-444-87109-1.50006-6).
- [11] H. Al-Wahsh, M. Urbán, and A. Czachor. Exact solutions for a model antiferromagnet with identical coupling between spins. *Journal of Magnetism and Magnetic Materials*, 185:L144–158, 6 1998. [doi:10.1016/S0304-8853\(97\)01147-5](https://doi.org/10.1016/S0304-8853(97)01147-5).
- [12] A. Czachor. Energy Spectrum for the System of N Ising Spins with Identical Spin-Spin Coupling K/N - Anatomy of Phase Transition. *Acta Physica Polonica A*, 113:1161–1169, 4 2008. [doi:10.12693/APhysPolA.113.1161](https://doi.org/10.12693/APhysPolA.113.1161).
- [13] J. E. Björnberg, J. Fröhlich, and D. Ueltschi. Quantum spins and random loops on the complete graph. *Communications in Mathematical Physics*, 375:1629–1663, 5 2020. [doi:10.1007/s00220-019-03634-x](https://doi.org/10.1007/s00220-019-03634-x).
- [14] M. Fannes, H. Spohn, and A. Verbeure. Equilibrium states for mean field models. *Journal of Mathematical Physics*, 21:355–358, 2 1980. [doi:10.1063/1.524422](https://doi.org/10.1063/1.524422).
- [15] K. Ryan. On a Class of Orthogonal-Invariant Quantum Spin Systems on the Complete Graph. *International Mathematics Research Notices*, 2023:6078–6131, 3 2023. [doi:10.1093/imrn/rnac034](https://doi.org/10.1093/imrn/rnac034).

[16] B. Tóth. Phase transition in an interacting Bose system. An application of the theory of Ventsel' and Freidlin. *Journal of Statistical Physics*, 61:749–764, 11 1990. [doi:10.1007/BF01027300](https://doi.org/10.1007/BF01027300).

[17] O. Penrose. Bose-Einstein condensation in an exactly soluble system of interacting particles. *Journal of Statistical Physics*, 63:761–781, 5 1991. [doi:10.1007/BF01029210](https://doi.org/10.1007/BF01029210).

[18] J. E. Björnberg. The free energy in a class of quantum spin systems and interchange processes. *Journal of Mathematical Physics*, 57, 7 2016. [doi:10.1063/1.4959238](https://doi.org/10.1063/1.4959238).

[19] G. Alon and G. Kozma. The mean-field quantum Heisenberg ferromagnet via representation theory. *Annales de l'Institut Henri Poincaré, Probabilités et Statistiques*, 57, 7 2021. [doi:10.1214/20-AIHP1067](https://doi.org/10.1214/20-AIHP1067).

[20] J. Björnberg, H. Rosengren, and K. Ryan. Heisenberg models and Schur–Weyl duality. *Advances in Applied Mathematics*, 151:102572, 10 2023. [doi:10.1016/j.aam.2023.102572](https://doi.org/10.1016/j.aam.2023.102572).

[21] N. Papanicolaou. Ground-state properties of spin-1 nematics. *Physics Letters A*, 116:89–93, 5 1986. [doi:10.1016/0375-9601\(86\)90246-X](https://doi.org/10.1016/0375-9601(86)90246-X).

[22] D. Jakab, G. Szirmai, and Z. Zimborás. The bilinear–biquadratic model on the complete graph. *Journal of Physics A: Mathematical and Theoretical*, 51:105201, 3 2018. [doi:10.1088/1751-8121/aaa92b](https://doi.org/10.1088/1751-8121/aaa92b).

[23] O. Ciftja, M. Luban, M. Auslender, and J. H. Luscombe. Equation of state and spin-correlation functions of ultrasmall classical Heisenberg magnets. *Physical Review B*, 60:10122–10133, 10 1999. [doi:10.1103/PhysRevB.60.10122](https://doi.org/10.1103/PhysRevB.60.10122).

[24] D. Loss and D. P. DiVincenzo. Quantum computation with quantum dots. *Physical Review A*, 57:120–126, 1 1998. [doi:10.1103/PhysRevA.57.120](https://doi.org/10.1103/PhysRevA.57.120).

[25] R. Woodworth, A. Mizel, and D. A. Lidar. Few-body spin couplings and their implications for universal quantum computation. *Journal of Physics: Condensed Matter*, 18:S721–S744, 5 2006. [doi:10.1088/0953-8984/18/21/S02](https://doi.org/10.1088/0953-8984/18/21/S02).

[26] J.-M. Liu and G. Müller. Dynamics of an integrable two-sublattice spin model with long-range interaction. *Physical Review B*, 44:12020–12022, 12 1991. [doi:10.1103/PhysRevB.44.12020](https://doi.org/10.1103/PhysRevB.44.12020).

[27] E. Magyari, H. Thomas, R. Weber, C. Kaufman, and G. Muller. Integrable and nonintegrable classical spin clusters. *Zeitschrift für Physik B Condensed Matter*, 65:363–374, 9 1987. [doi:10.1007/BF01303725](https://doi.org/10.1007/BF01303725).

[28] G. Müller. High-temperature spin dynamics of the classical Heisenberg magnet in one, two, three and infinite dimensions. *Le Journal de Physique Colloques*, 49:C8–1403–C8–1404, 12 1988. [doi:10.1051/jphyscol:19888644](https://doi.org/10.1051/jphyscol:19888644).

[29] R. Dekeyser and M. H. Lee. Time-dependent correlations for spin Van der Waals systems. *Physical Review B*, 19:265–273, 1 1979. [doi:10.1103/PhysRevB.19.265](https://doi.org/10.1103/PhysRevB.19.265).

[30] M. H. Lee, I. M. Kim, and R. Dekeyser. Time-Dependent Behavior of the Spin-½ Anisotropic Heisenberg Model in Infinite Lattice Dimensions. *Physical Review Letters*, 52:1579–1582, 4 1984. [doi:10.1103/PhysRevLett.52.1579](https://doi.org/10.1103/PhysRevLett.52.1579).

[31] V. G. Drinfeld. *Quantum Groups*, in *Proc. Int. Congr. Math. (Berkeley 1986)*, pages 798–820. American Mathematical Society, 1987.

[32] M. Jimbo. A q -Difference Analogue of $U(g)$ and the Yang-Baxter Equation. *Letters in Mathematical Physics*, 10:63–69, 7 1985. [doi:10.1007/BF00704588](https://doi.org/10.1007/BF00704588).

[33] E. K. Sklyanin. Boundary conditions for integrable quantum systems. *Journal of Physics A: Mathematical and General*, 21:2375–2389, 5 1988. [doi:10.1088/0305-4470/21/10/015](https://doi.org/10.1088/0305-4470/21/10/015).

[34] V. Pasquier and H. Saleur. Common structures between finite systems and conformal field theories through quantum groups. *Nuclear Physics B*, 330:523–556, 1 1990. [doi:10.1016/0550-3213\(90\)90122-T](https://doi.org/10.1016/0550-3213(90)90122-T).

[35] C. Gómez, M. Ruiz-Altaba, and G. Sierra. Quantum groups in two-dimensional physics. *Quantum Groups in Two-Dimensional Physics*, page 475, 1996.

[36] P. P. Kulish and E. K. Sklyanin. The general $U_q(\mathfrak{sl}(2))$ invariant XXZ integrable quantum spin chain. *Journal of Physics A: Mathematical and General*, 24:L435–L439, 4 1991. [doi:10.1088/0305-4470/24/8/009](https://doi.org/10.1088/0305-4470/24/8/009).

[37] P. Martin and H. Saleur. On an algebraic approach to higher dimensional statistical mechanics. *Communications in mathematical physics*, 158(1):155–190, 1993.

[38] P. Martin and H. Saleur. The blob algebra and the periodic Temperley-Lieb algebra. *Letters in mathematical physics*, 30(3):189–206, 1994.

[39] J. Lamers, V. Pasquier, and D. Serban. Spin-Ruijsenaars, q -Deformed Haldane-Shastry and Macdonald Polynomials. *Communications in Mathematical Physics*, 393:61–150, 7 2022. [doi:10.1007/s00220-022-04318-9](https://doi.org/10.1007/s00220-022-04318-9).

[40] T. Hakobyan and A. Sedrakyan. Spin chain Hamiltonians with affine $U_q g$ symmetry. *Physics Letters B*, 377:250–254, 6 1996. [doi:10.1016/0370-2693\(95\)01320-2](https://doi.org/10.1016/0370-2693(95)01320-2).

[41] M. Matushko and A. Zotov. Elliptic generalisation of integrable q -deformed anisotropic Haldane-Shastry long-range spin chain. *Nonlinearity*, 36:319–353, 1 2023. [doi:10.1088/1361-6544/aca510](https://doi.org/10.1088/1361-6544/aca510).

[42] R. Klabbers and J. Lamers. The deformed Inozemtsev spin chain. *SciPost Physics*, 17:155, 12 2024. [doi:10.21468/SciPostPhys.17.6.155](https://doi.org/10.21468/SciPostPhys.17.6.155).

[43] S. Majid. *Foundations of Quantum Group Theory*. Cambridge University Press, 12 1995. [doi:10.1017/CBO9780511613104](https://doi.org/10.1017/CBO9780511613104).

[44] L. C. Biedenharn and M. A. Lohe. *Quantum Group Symmetry and Q-Tensor Algebras*. World Scientific, 8 1995. [doi:10.1142/2815](https://doi.org/10.1142/2815).

[45] T. L. Curtright, G. I. Ghandour, and C. K. Zachos. Quantum algebra deforming maps, Clebsch–Gordan coefficients, coproducts, R and U matrices. *Journal of Mathematical Physics*, 32:676–688, 3 1991. [doi:10.1063/1.529410](https://doi.org/10.1063/1.529410).

[46] D. Bonatsos and C. Daskaloyannis. Quantum groups and their applications in nuclear physics. *Progress in Particle and Nuclear Physics*, 43:537–618, 1 1999. [doi:10.1016/S0146-6410\(99\)00100-3](https://doi.org/10.1016/S0146-6410(99)00100-3).

[47] A. Ballesteros and S. M. Chumakov. On the spectrum of a Hamiltonian defined on $SU_q(2)$ and quantum optical models. *Journal of Physics A: Mathematical and General*, 32:6261–6269, 9 1999. [doi:10.1088/0305-4470/32/35/305](https://doi.org/10.1088/0305-4470/32/35/305).

[48] Z. Chang and H. Yan. The $SU_q(2)$ quantum group symmetry and diatomic molecules. *Physics Letters A*, 154:254–258, 4 1991. [doi:10.1016/0375-9601\(91\)90816-Q](https://doi.org/10.1016/0375-9601(91)90816-Q).

[49] M. R. Ubriaco. Thermodynamics of a free $SU_q(2)$ fermionic system. *Physics Letters A*, 219:205–211, 8 1996. [doi:10.1016/0375-9601\(96\)00446-X](https://doi.org/10.1016/0375-9601(96)00446-X).

[50] M. R. Ubriaco. λ -transition in low dimensional systems with $SU_q(2)$ symmetry. *Physics Letters A*, 241:1–6, 4 1998. [doi:10.1016/S0375-9601\(98\)00149-2](https://doi.org/10.1016/S0375-9601(98)00149-2).

[51] M. R. Ubriaco. Geometry of quantum group invariant systems. *Physics Letters A*, 376:3581–3587, 11 2012. [doi:10.1016/j.physleta.2012.10.042](https://doi.org/10.1016/j.physleta.2012.10.042).

[52] A. Ballesteros, O. Civitarese, F. J. Herranz, and M. Reboiro. Fermion-boson interactions and quantum algebras. *Physical Review C*, 66:064317, 12 2002. [doi:10.1103/PhysRevC.66.064317](https://doi.org/10.1103/PhysRevC.66.064317).

[53] A. Ballesteros, I. Gutierrez-Sagredo, V. Mariscal, and J. J. Relancio. Quantum group deformation of the Kittel–Shore model. *Journal of Physics A: Mathematical and Theoretical*, 58(44):445202, oct 2025. [doi:10.1088/1751-8121/ae1272](https://doi.org/10.1088/1751-8121/ae1272).

[54] A. Ballesteros and O. Ragnisco. A systematic construction of completely integrable Hamiltonians from coalgebras. *Journal of Physics A: Mathematical and General*, 31:3791–3813, 4 1998. [doi:10.1088/0305-4470/31/16/009](https://doi.org/10.1088/0305-4470/31/16/009).

[55] P. M. Morse. The Theory of Electric and Magnetic Susceptibilities. By J. H. van Vleck. Oxford University Press, 384 pages, 1932. *Science*, 76:326–328, 10 1932. [doi:10.1126/science.76.1971.326](https://doi.org/10.1126/science.76.1971.326).

[56] M. Kac. Statistical physics, phase transitions and superfluidity. *Brandeis University Summer Institute in Theoretical Physics*, 1:241–305, 1968.

[57] C. Kittel. *Introduction to Solid State Physics*. John Wiley & Sons, 2005.

[58] A. J. Ferguson, P. A. Cain, D. A. Williams, and G. A. D. Briggs. Ammonia-based quantum computer. *Physical Review A*, 65:034303, 2 2002. [doi:10.1103/PhysRevA.65.034303](https://doi.org/10.1103/PhysRevA.65.034303).

[59] O. Ciftja. The irregular tetrahedron of classical and quantum spins subjected to a magnetic field. *Journal of Physics A: Mathematical and General*, 34:1611–1627, 3 2001. [doi:10.1088/0305-4470/34/8/308](https://doi.org/10.1088/0305-4470/34/8/308).

[60] O. Ciftja. Spin correlation functions of some frustrated ultra-small classical Heisenberg clusters. *Physica A: Statistical Mechanics and its Applications*, 286:541–557, 11 2000. [doi:10.1016/S0378-4371\(00\)00326-5](https://doi.org/10.1016/S0378-4371(00)00326-5).

[61] P. Sheng, R. W. Cohen, and J. R. Schrieffer. Melting transition of small molecular clusters. *Journal of Physics C: Solid State Physics*, 14:L565–L569, 7 1981. [doi:10.1088/0022-3719/14/20/001](https://doi.org/10.1088/0022-3719/14/20/001).

[62] S. M. Sandoval, A. E. Sepulveda, and S. M. Keller. On the thermodynamic efficiency of a nickel-based multiferroic thermomagnetic generator: From bulk to atomic scale. *Journal of Applied Physics*, 117, 4 2015. [doi:10.1063/1.4919354](https://doi.org/10.1063/1.4919354).

[63] C.-J. Hsu, S. M. Sandoval, K. P. Wetzel, and G. P. Carman. Thermomagnetic conversion efficiencies for ferromagnetic materials. *Journal of Applied Physics*, 110, 12 2011. [doi:10.1063/1.3672844](https://doi.org/10.1063/1.3672844).

[64] C. Q. Sun, W. H. Zhong, S. Li, B. K. Tay, H. L. Bai, and E. Y. Jiang. Coordination Imperfection Suppressed Phase Stability of Ferromagnetic, Ferroelectric, and Superconductive Nanosolids. *The Journal of Physical Chemistry B*, 108:1080–1084, 1 2004. [doi:10.1021/jp0372946](https://doi.org/10.1021/jp0372946).

[65] H. Al-Wahsh, D. Bria, A. Akjouj, and P. Zieliński. Nonlinear effect of perpendicular magnetic field on the antiferromagnetic phase transition in weakly coupled layered systems: Equal access decoupling scheme. *Physical Review B*, 70:014405, 7 2004. [doi:10.1103/PhysRevB.70.014405](https://doi.org/10.1103/PhysRevB.70.014405).

[66] H. Al-Wahsh, G. Ismail, and K. Lotfy. Extended random phase approximation for layered copper oxides antiferromagnets. *Czechoslovak Journal of Physics*, 54:1511–1520, 12 2004. [doi:10.1007/s10582-004-1208-7](https://doi.org/10.1007/s10582-004-1208-7).

[67] C. Gros, W. Wenzel, and J. Richter. The Transition from an Ordered Antiferromagnet to a Quantum Disordered Spin Liquid in a Solvable Bilayer Model. *Europhysics Letters (EPL)*, 32:747–752, 12 1995. [doi:10.1209/0295-5075/32/9/008](https://doi.org/10.1209/0295-5075/32/9/008).

[68] A. Czachor and H. Al-Wahsh. Green's function approach to the neutron-inelastic-scattering determination of magnon dispersion relations for isotropic disordered magnets. *Physical Review B*, 63:064419, 1 2001. [doi:10.1103/PhysRevB.63.064419](https://doi.org/10.1103/PhysRevB.63.064419).